

Research report:

Influence of various admixture/aggregates on environmental, mechanical and durability properties of cementitious building materials

Investigation on Hybrid Fiber-Reinforced Concrete



Marshallplan-Jubiläumsstiftung

Austrian Marshall Plan Foundation



Submitted by:

Dipl. Ing. Marcus Maier

Supervisor:

Univ. Prof. Claudia P. Ostertag

Department of Civil & Environmental Engineering

University of California, Berkeley, USA

Table of Contents

1	Introduction.....	4
2	Mechanical and durability characteristics of hybrid fiber-reinforced concrete	4
3	Introduction to Self-Sensing-Properties	7
3.1	Structural health monitoring (SHM).....	7
4	State of Arts on Self-Sensing Concrete.....	7
4.1	Electrochemical fundamentals.....	8
4.1.1	Electrical resistance	8
4.1.2	Electrical conductivity.....	8
4.1.3	Piezoresistive materials	9
4.1.4	Polarization.....	9
4.2	Measurement Methods and Data Presentation	10
4.2.1	Two – and Four probe method	10
4.2.2	Direct Current (DC) and Alternating Current (AC).....	11
4.2.3	AC-Circuit Theory.....	11
4.2.4	Electrical Impedance Spectroscopy (EIS)	14
4.2.5	Gauge factor	17
4.2.6	Fundamentals of Potentiostat – EIS- Measurement techniques	17
4.3	Types of electrodes	23
4.3.1	Embedded electrodes.....	23
4.3.2	Surface electrodes.....	23
4.4	Influence of additives and curing properties	25
4.4.1	Hydration time	25
4.4.2	Temperature	25
4.4.3	Sand/cement ratio	26
4.4.4	Gravel/sand ratio	27
4.5	Functional fillers	28
4.5.1	Steel.....	28
4.5.2	Carbon.....	29
4.5.3	Carbon Nano Tubes	31
4.5.4	Graphene.....	32
4.5.5	Overview of self-sensing research	33
5	Experimental method	36
5.1	Material properties	36

5.2	Test specification	36
6	Results	38
6.1	Stability pre-test.....	38
6.2	Stability measurement before bending test.....	40
6.3	Bending test and Impedance measurement	42
7	Conclusion	47
8	Acknowledgement.....	47
9	References	47

1 Introduction

Civil engineering has a longstanding tradition in the design of building materials for structures, buildings and infrastructures with respect to optimized material behavior. The mechanical properties of structural building materials have reached a high optimized level. Due to the increasing costs and the huge carbon footprint at the manufacturing process of cement a change of requirements besides enhancing mechanical properties become relevant. Nowadays, very high technical specifications shift from exclusively mechanical properties towards an optimized mix of mechanical and safety-performance through durability and sustainability of cementitious building materials.

Furthermore, assessment and damage monitoring of existing buildings is of high interest to maintain safety levels and to reduce maintenance costs. This is done with high effort and time consuming periodical inspections of structures. Currently those inspections are done visually or with intense measurement instrumentation – the so called structural health monitoring. To reduce this high expenditure, smart structural materials which monitor themselves without embedded or attached sensors could facilitate inspections and reduce maintenance costs. Those self-sensing materials could e.g. track crack propagation and therefore monitor damage level of the structure.

As a matter of fact, mechanical, safety and durability enhancement of building materials combined with the implementation of self-sensing properties is still at its beginning of civil engineering applications. However, increased flexibility in the production process of materials and in the choice of constituents provides the proper basis for the performance-oriented design of materials. This enables the improvement of mechanical properties, durability enhancement combined with self-sensing properties.

Within this project the self-sensing properties of a concrete mixture with enhanced mechanical and durability properties is investigated. A combination of these benefits could provide in-situ information of the concrete structure and therefore enables long-term monitoring and safety assessments. For this purpose a Hybrid Fiber-Reinforced Concrete mixture (HyFRC) developed by Prof. Claudia P. Ostertag at the University of California, Berkeley is used to employ a self-sensing measurement method and furthermore to investigate its self-sensing properties.

2 Mechanical and durability characteristics of hybrid fiber-reinforced concrete

The challenges which have to be faced by designing new concrete mixtures to meet the above mentioned properties are a) to eliminate the brittle behavior of ordinary concrete and therefore enhance strength performance b) reduce cracking to minimize intrusion of chlorides or carbon dioxide which damages the concrete matrix and c) increase the conductivity of concrete to enable self-sensing properties. Previous studies showed the beneficial effect of combining different types of fibers (Jen, Trono, & Ostertag, 2016; Nemkumar Banthia & Sayed Mohamad Soleimani). When considering material durability, a hybrid combination of steel and polyvinyl alcohol (PVA) fibers showed a beneficial effect of higher propensity of multiple cracking (John S. Lawler). Within this mixture, the macro fibers (Steel) change the material properties from brittle to ductile where the micro fibers (PVA) increase the maximum load and sustain fictional slip of the macro fibers upon pullout (Markovich I, Van Mier J.G., & Walraven J.C, 2001) This combination allows the material to form multiple cracks instead of dominated larger cracks.

These beneficial effects were chosen by Professor C. P. Ostertag and her research group at the University of California, Berkeley to develop and investigate a concrete mixture which meets the above mentioned criteria of enhanced mechanical behavior and self-sensing properties.

An experimental investigation was conducted to evaluate the mechanical characteristics of Hybrid fiber-reinforced concrete (HyFRC). This was done by varying the amount of steel and PVA fibers and the obtained mechanical performance was compared by conducting four-point bending tests. Figure 1 shows the experimental setup for bending tests and the specimen sizes (J. Blunt & Ostertag, 2009).

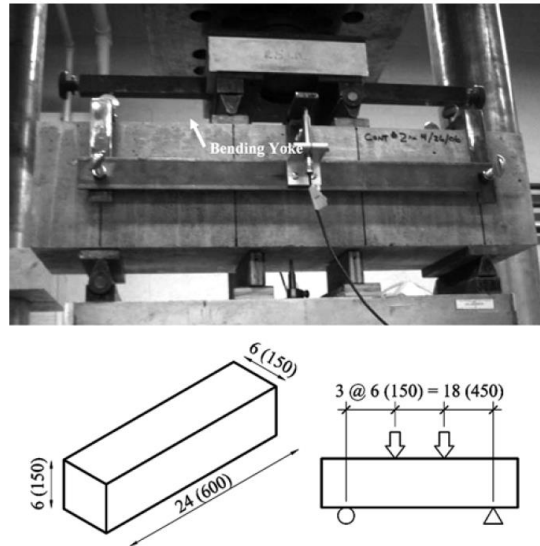


Figure 1: Specimen size and experimental setup for bending tests (J. Blunt & Ostertag, 2009)

Table 1 presents the investigated concrete mixtures and their fiber contents. Five mixtures were investigated with a variation of PVA and steel fiber content. PVA fibers with a length of 8 mm and two different steel fibers with 30 and 60 mm length were used for investigation. All fiber properties are given in Table 2.

Table 1: Selected concrete mixtures for mechanical investigation (J. Blunt & Ostertag, 2009)

Trail batch	Maximum aggregate size (mm)	Fiber volume fraction %		
		PA	S1 (30mm)	S2 (60mm)
F1	25	-	-	0.7
F2	25	0.3	-	0.7
F3	25	0.3	-	0.7
F4	9.5	0.2	0.5	0.5
F5	9.5	0.2	0.5	0.8

Table 2: Fiber properties for experimental study (J. Blunt & Ostertag, 2009)

Designation	Material	Length (mm)	Diameter (mm)	Strength (MPa)	Stiffness (GPa)
PA	PVA	8	0.04	1600	42
S1	Steel, hooked	30	0.55	1100	200
S2(1)	Steel, hooked	60	0.92	1050	200
S2(2)	Steel, hooked	60	0.75	1050	200

Mixture F1 represents a fiber-reinforced concrete (FRC) with 60 mm long steel fibers resulting in a typically FRC flexural behavior as shown in Figure 2. This is characterized by a linear elastic behavior up to matrix cracking strength followed by a drop of load capacity due to crack formation. Adding a small amount of 0.3 Vol% of PVA fibers (Mixture F2) reduces the load drop at first peak. Mixture F3 consists of the same amount of PVA and steel fibers as Mixture F2 only steel fibers with a reduced diameter of 0.75 instead of 0.92 mm were used. This smoothed the transition from the matrix cracking strength to peak flexural load. To push the flexural load capacity to a higher level steel fibers with a length of 30 mm was added to the mixture F4. This mixture contained 0.2 Vol% of PVA and 0.5 Vol% of both 30 and 60 mm steel fibers. By raising the amount of 60 mm steel fibers from 0.5 to 0.8 Vol% a higher maximum flexural strength was reached (see Figure 2).

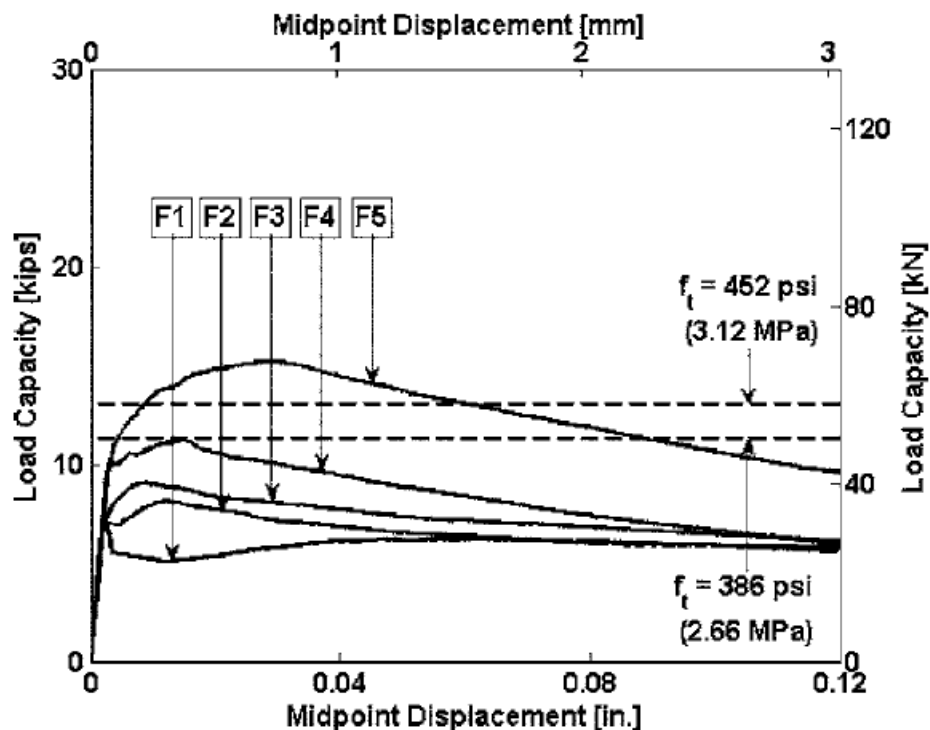


Figure 2: Flexural behavior of investigated mixtures (J. Blunt & Ostertag, 2009)

This mixture will be used to verify its self-sensing properties and assess its application field for self-monitoring measurements.

The report will start off with a state of the arts of self-sensing concrete technology, how to conduct resistance measurement and highlight measurement benefits and drawbacks. The main emphasis of this part is the fundamental principles of self-sensing concrete, their influence on electrical resistivity and measurement of the change in electrical resistance during loading. This is followed by an introduction to the used measurement technique – the Potentiostat and Electrochemical Impedance Measurement (EIS). Finally the obtained findings were applied to conduct self-sensing measurements during bending tests on a HyFRC mixture. During bending test micro and macro cracks form and therefore damage the cross section of the specimen. This effect will be compared with the self-sensing measurement results to evaluate the method's usability of damage detection during testing.

3 Introduction to Self-Sensing-Properties

3.1 Structural health monitoring (SHM)

Self-sensing concrete provides a real-time damage and deterioration monitoring of a structure. Traditional strain gauges generally used these days for structural health monitoring (SHM) have several shortcomings. For instance, difficulties in long-term reliability, low anti-electromagnetic interference, and less accuracy for long term monitoring (Han, Guan, & Ou, 2006). Self-sensing concrete based on piezoresistive measurements can also capture a larger area to be considered compared to traditional strain gauge acting as a point based sensor. A point based sensor detects only local damages for specific zones of interest which can be defined as critical measurement accuracy in the structure (Ranade, Zhang, Lynch, & Li, 2014).

Despite those facts, self-sensing concrete is not widely used today for SHM. This can be explained by all the internal and external factors which influence the electrical resistivity. Factors which influence sensitivity for SHM. More research and greater knowledge within this field are necessary before the full potential of this technology can be adopted by the SHM industry.

4 State of Arts on Self-Sensing Concrete

This chapter will first go through the fundamental principles of self-sensing concrete with the focus on electrical resistance, piezoresistivity, electrical conduction in cementitious composites, the polarization effect and different methods for measuring the electrical resistance. Furthermore a more detailed insight of factors influencing electrical resistivity and different functional fillers will be given. In general, according to (Han, Ding, & Yu, 2014), the following parameter primary influence the electrical resistivity of concrete:

- Functional filler concentration
- Functional filler geometrical shape
- Loading Rate
- Water Content
- Temperature
- Freeze-thaw cycle
- Dry-wet cycle
- Corrosive environment

4.1 Electrochemical fundamentals

To understand the functionality of self-sensing concrete and their influencing parameter knowledge of electricity and electrochemical fundamentals is recommended. The following chapter will serve as an overview of basics needed to understand self-sensing measurements and properties.

4.1.1 Electrical resistance

An electrical resistance of a circuit element is the ability to resist the flow of electrical current. According to Ohm's Law, the resistance (R) in ohm is defined as the ratio between voltage (V) in volt and current (I) in ampere:

$$R = \frac{V}{I}$$

Furthermore, it is important to point out the difference between electrical resistance and resistivity. Electrical resistance is dependent on the geometrical shape, while, the electrical resistivity is independent of geometrical shape, and can be used to compare electrical properties of different materials (Azhari, 2008). The concrete resistivity is influenced by many factors, and therefore the resistivity between concrete mixtures should not directly be compared without taking these factors into account. Electrical resistivity ρ in Ohm-m is calculated by the following expression:

$$\rho = R \frac{A}{L}$$

where R is the electrical resistance in ohm, A is the cross-sectional area in m², and L is the distance between the electrodes in m.

Moreover, the cross-sectional area (A) varies on the measurement method, e.g. it can be assumed to be the whole cross-section when using mesh or plate electrodes which have the equivalent area than the specimen cross-section. Hence, the electrical resistivity cannot that easily be determined when using surface electrodes, such as line and loop electrodes, because of the uncertainty of current penetration and flow path into the specimen. Different types of electrodes will be described in more detail in chapter 4.3.

4.1.2 Electrical conductivity

The electrical conductivity σ with its SI-Unit Siemens/meter of a material is expressed by the inverse resistivity:

$$\sigma = \frac{1}{\rho}$$

where σ is the conductivity and ρ is the resistivity.

According to (Han, Yu, & Ou, 2014), the conduction of self-sensing cementitious materials is complex due to several types of electrical conduction phenomena that act simultaneously. These types of

electrical conduction can be categorized into the following main groups: Electronic and conduction & Ionic conduction.

Electronic and conduction can be divided into the following subgroups: Contact conduction, tunnel conduction and field emission conduction, and all of them are related to the functional filler. For instance, contact conduction can be considered as a conductive network provided by the steel or carbon fibers while ionic conduction is related to the matrix. This type of conduction causes the polarization effect.

The **ionic conduction** can be reduced by removing pore water. Then electrical conductivity is provided only by the functional filler and can be determined more accurately.

According to (Wen & Chung, 2000), plain cement paste (cement and water) without any functional fillers can also be used for damage monitoring by electrical resistance measurement. Their findings indicate that only ionic conduction is sufficient for providing self-sensing properties.

4.1.3 Piezoresistive materials

In a piezoresistive material the electrical resistivity changes because of an applied stress or strain. The applied stress/strain cause the atomic structure in the material to change, and therefore the electrical resistivity will also change for a conductive material. The change in electrical resistivity of concrete can be explained by the change in atomic structure of conductive components, but also by cracks during loading which cause a change of the conductive network. Because of this behavior, concrete can be categorized as a piezoresistive material when there is a sufficient conductivity. It is the piezoresistive property that makes the concrete self-sensing by applying an electrical potential to the material during loading and then measure the change electrical resistance. There are several different components in the concrete that provide conductivity, such as ions in the pore water and other cement-based conductive materials. Moreover, the piezoresistivity depends on many factors that will be elaborated later in this paper. In general, by adding cement-based piezoresistive materials to the concrete or the mortar mixture, the sensitivity increases. Cement-based piezoresistive materials, such as conductive fiber and particles, will further be defined as functional fillers.

4.1.4 Polarization

The polarization effect is a result of ions moving in the pore water such as Na^+ , Ca^+ , Ca^{2+} & OH^- (Han, Yu, et al., 2014). When applying a potential (voltage) to the concrete these ions create a conductive network between the capillary pores, where the positive ions will move to the negative electrode, and the negative ions will move to the positive electrode. The movement of ions toward electrodes is illustrated in Figure 3. The polarization of ions will then create a potential that is opposite of the applied potential, and the measured resistivity will increase (Azhari, 2008). DC or low-frequency (Hz) AC measurements are more often influenced by the polarization effect, and it is recommended to take preventive actions to either reduce the polarization effect or adjust the measurements after the loading sequence (Hou & Lynch, 2005).

The polarization effect can be reduced by applying the voltage ahead of the loading sequence which will then cause the polarization effect to plateau off (Han, Yu, et al., 2014). Another option is to measure the change resistance due to polarization for an unload specimen, and then adjust the results for the loaded specimen (Hou & Lynch, 2005). According to (Hou & Lynch, 2005), the polarization effect is reduced to an acceptable level by using AC with a high frequency. An alternating cur-

rent (AC) reduce the polarization effect because the electrodes change direction as the current shifts with the frequency (Solgaard, Geiker, Edvardsen, & Kuter, 2013).

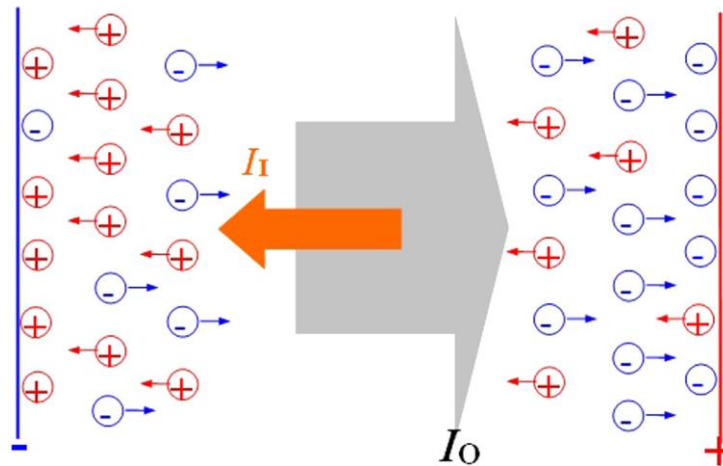


Figure 3: Polarization (Han, Yu, et al., 2014)

4.2 Measurement Methods and Data Presentation

4.2.1 Two – and Four probe method

Two different methods are common for measuring the electrical resistance in concrete. In the two-probe method, both the electrical current and voltage electrode enter the specimen at the same electrode. While, in the four-probe method, the voltage and current electrode enters at two different probes. The current electrode enters the specimen in the outer probes, and the voltage drop is measured at the inner electrodes, as illustrated in Figure 4.

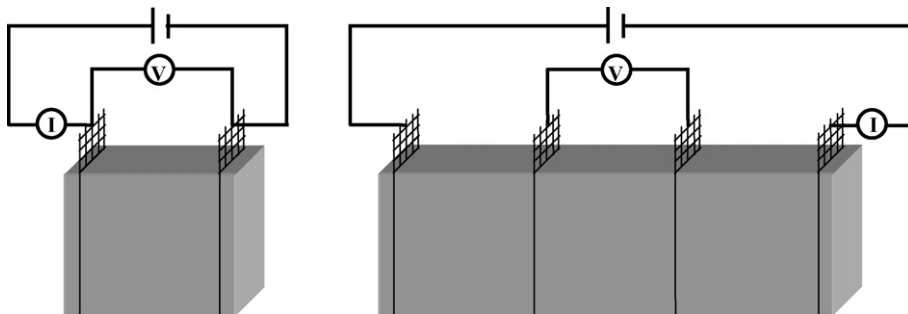


Figure 4: Overview of Two and Four-probe method (Han et al., 2006)

Another option is to measure the electrical resistance by a potentiostat containing several electrodes with different functions. This method can also be conducted either with two or four probes entering the specimen. Figure 5 illustrates measurements for a two and four-probe method with a

potentiostat configuration with working (W), Sense (S), Counter (C), and Reference (R) electrodes. Chapter 4.2.6 describes this potentiostat configuration in more detail.

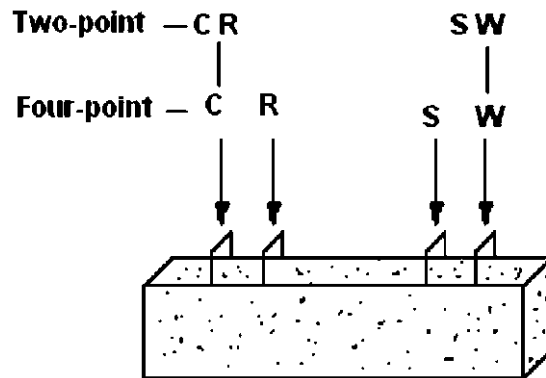


Figure 5: Overview of Two and Four-probe method configuration with a Potentiostat (Chiarello & Zinno, 2004)

4.2.2 Direct Current (DC) and Alternating Current (AC)

The electrical resistance can be measured either by applying a direct current (DC) or an alternating current (AC). DC is the simplest method for measuring electrical resistance because the applied voltage is fixed and the conventional Ohm's Law can be used to determine the electrical resistance. However, DC measurements are more influenced by the polarization effect, therefore considered as less accurate compared to the AC method as mentioned in chapter 4.1.4.

AC is a more complex method because the current follows a sinusoidal response, and the impedance (resistance) is represented by a complex number with a real and an imaginary part. Because the AC method is considered as more accurate, this method was selected for the four-point bending test experiment that will be presented in chapter 5.

4.2.3 AC-Circuit Theory

An electrical resistance of a circuit element has the ability to resist the flow of electrical current. According to Ohm's Law the resistance is defined as the ratio between voltage (E) and current (I) as followed:

$$R = \frac{E}{I}$$

This relationship is limited to only one circuit element known as ideal resistor. An Ideal resistor has several simplifying properties:

- It follows Ohm's Law at all current and voltage levels
- It's resistance value is independent of frequency
- Alternating current (AC) and voltage signals through a resistor are in phase with each other

These simplified properties are not appropriate for more complex circuits and therefore a more general circuit parameter – impedance – was introduced. Impedance and resistance are a measure

of the ability of a circuit to resist the flow of electrical current. However, impedance is not limited by the simplifying properties listed above.

Electrochemical impedance is usually measured by applying an AC potential (e.g.: sinusoidal potential excitation) to an electrochemical cell and measuring the current through the cell. The response of this signal is a AC current signal, containing the excitation frequency and it's harmonics. The current signal can be analyzed as a sum of sinusoidal functions (a Fourier series) (GAMRY-TUT-1, 2015).

Additionally, electrochemical impedance measurement uses a small excitation signal which leads to a pseudo-linear response of the cell (Figure 11). The Current response in a linear sinusoidal potential system will be a sinusoid at the same frequency but shifted in phase (Figure 6).

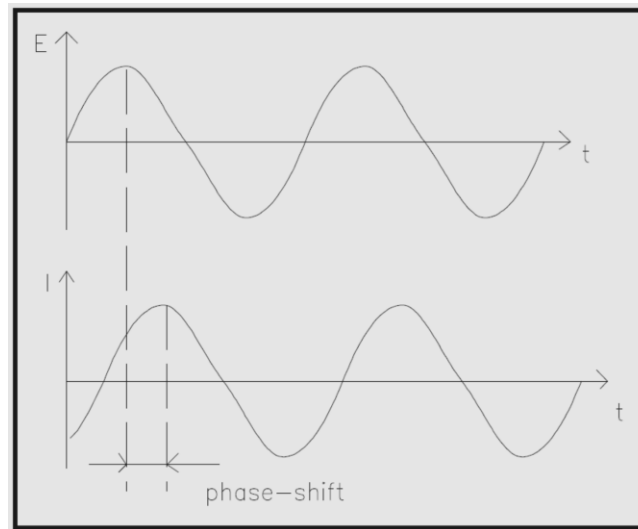


Figure 6: Sinusoidal Current Response in a Linear System

The excitation signal, expressed as a function of time has the form:

$$E_t = E_0 \sin(\omega t)$$

$E(t)$ is the potential at time t , E_0 is the amplitude of the signal, and ω is the radial frequency. The relationship between radial frequency ω and frequency f is expressed as:

$$\omega = 2 \pi f$$

In a linear system, the response signal is shifted in phase φ and has a different amplitude I_0 :

$$I(t) = I_0 \cos(\omega t - \varphi)$$

An expression analogous to Ohm's Law allows expressing the impedance of the system as:

$$Z = \frac{E(t)}{I(t)} = \frac{E_0 \cos(\omega t)}{I_0 \cos(\omega t - \varphi)} = Z_0 \frac{\cos(\omega t)}{\cos(\omega t - \varphi)}$$

The impedance is therefore represented in terms of a magnitude, Z_0 and a phase shift φ . Another way to express the impedance is by using Euler's relationship,

$$e^{j\varphi} = \cos(\varphi) + j \sin(\varphi)$$

It is possible to express the impedance as a complex function, which leads to potential

$$E(t) = E_0 e^{j\omega t}$$

And the current response

$$I(t) = I_0 e^{j\omega t - j\varphi}$$

The impedance is then represented as a complex number, written as:

$$Z = \frac{E}{I} = Z_0 e^{j\varphi} = Z_0(\cos\varphi + j \sin\varphi)$$

And can be separated in a real and an imaginary part.

If the applied sinusoidal signal on the X-axis of a graph and the sinusoidal response signal $I(t)$ on the Y-axis is plotted, an oval is pictured (see Figure 7). This oval is known as a "Lissajous figure". Analysis of Lissajous figures on oscilloscope screens was the accepted method of impedance measurement prior to the availability of lock-in amplifiers, frequency response analyzers, and digital signal processing.

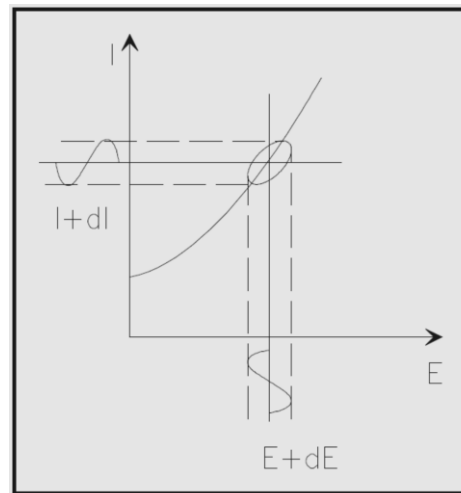
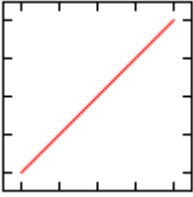
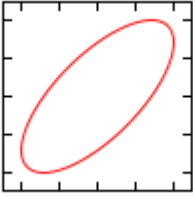
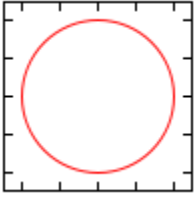
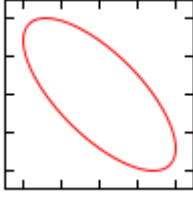
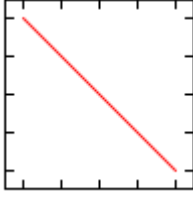
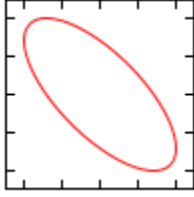
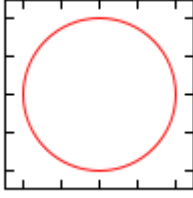
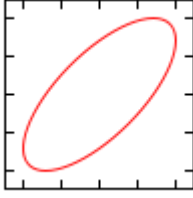
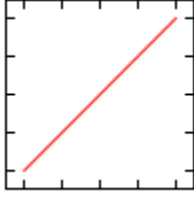


Figure 7: Origin of Lissajous Figure

For a better understanding of the Lissajous figures – which are shown during the measurement of the EIS-system used for the later experimental method - . (GAMRY-APN-1, 2015)

Table 3 shows the most common resultant figures of a frequency-ratio of 1:1 and their shift in phase during EIS Measurement (GAMRY-TUT-1, 2015). (GAMRY-APN-1, 2015)

Table 3: Lissajouse figures at Frequency ratio of 1:1 and different Phase-shift

$\Delta\phi$	0	$\frac{1}{4}\pi$	$\frac{1}{2}\pi$
Freq. ratio: 1:1			
$\Delta\phi$	$\frac{3}{4}\pi$	1π	$1\frac{1}{2}\pi$
Freq. ratio: 1:1			
$\Delta\phi$	$1\frac{1}{2}\pi$	$1\frac{3}{4}\pi$	2π
Freq. ratio: 1:1			

4.2.4 Electrical Impedance Spectroscopy (EIS)

For the experimental method used for chapter 5 an EIS was conducted at a frequency range from 1 mHz to 100kHz. The bending test then was conducted at 100 kHz to measure the change in impedance during loading. This subchapter will provide a solid background of EIS-Data presentation and fundamentals of a Potentiostat.

EIS-Data Presentation

The Results of an EIS measurement are showed in a Nyquist and Bode plot. For the **Nyquist plot** the real part is plotted on the X - Axis and the imaginary part on the Y-Axis as shown in Figure 8. It should be mentioned that the Imaginary part (Y-Axis) is negative and each point of the Nyquist plot represents an impedance of one frequency. The right part of the graph represents low frequencies and high frequencies are shown on the left side. This is true for EIS data where impedance usually falls as frequency rises but is not true for all circuits. The impedance can be represented as a vector of length $|Z|$. The angle between this vector and the X-axis is ϕ , which is known as the phase shift between the applied voltage and measured current. This plot however has a shortcoming namely the recorded frequency of each point cannot be seen. Figure 8 results from an electrical circuit of Figure 9, which its semicircle is characteristic for a single "time constant". Electrochemical Imped-

ance plots often contain several time constant and only just a portion of one or more of their semi-circles is seen due to the measurements limit on frequency range (GAMRY-APN-3, 2015).

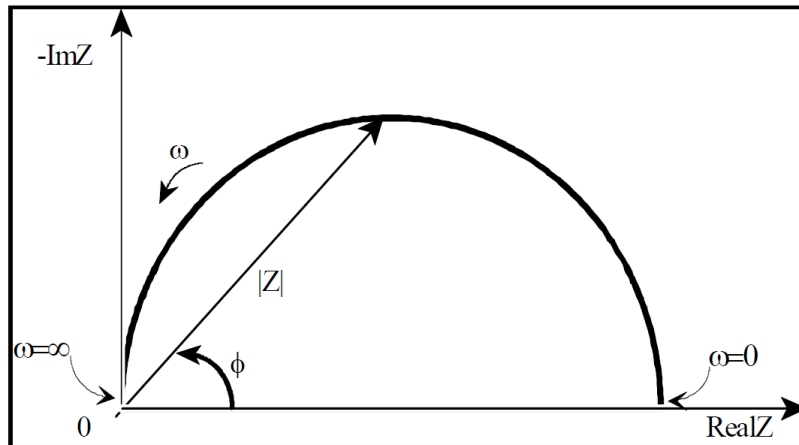


Figure 8: Nyquist plot

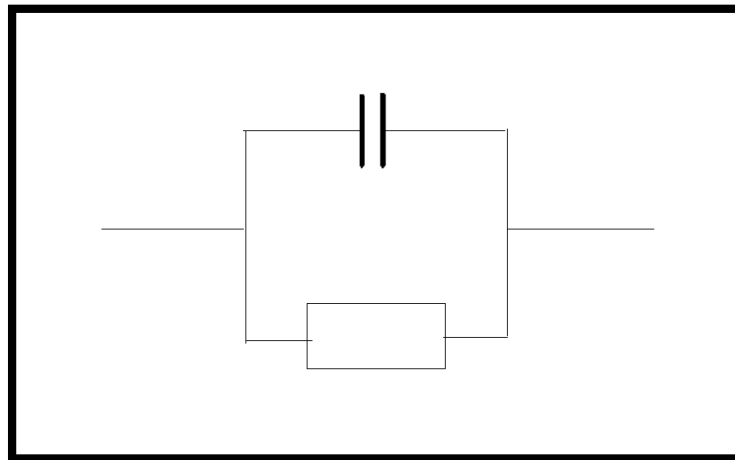


Figure 9: Simple Equivalent Circuit with One Time Constant

Another popular presentation method is the Bode plot where the impedance is plotted with log frequency on the X-axis and both the absolute value of the impedance, $\log |Z|$ and phase-shift, ϕ , on the Y-axis. The bode plot of the circuit of Figure 9 is shown in Figure 10. Unlike the Nyquist plot, the Bode plot explicitly shows the frequency information (GAMRY-TUT-1, 2015).

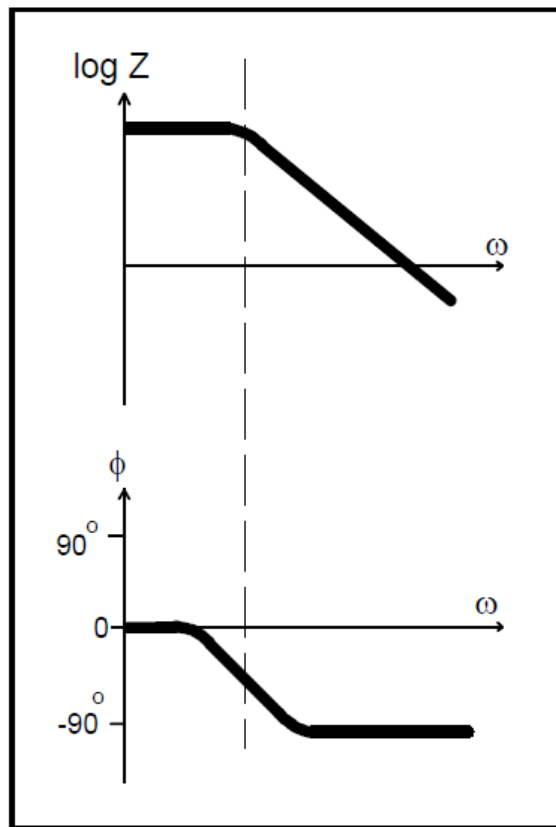


Figure 10: Bode Plot with One Time Constant

Usage of small voltage for linearity

Impedance analysis of linear circuits is much easier than those of non-linear systems, but electrochemical cells are not linear as shown in Figure 11. Remind, for an electrochemical cell the input is the potential and the output the current, furthermore doubling the voltage will not necessarily double the current. In EIS practice only a small AC signal (1 to 10 mV) is applied to the cell to ensure a small enough measurement region, a so called “pseudo-linear” segment in a current versus voltage curve where linearity can be assumed (Figure 11) (GAMRY-TUT-1, 2015).

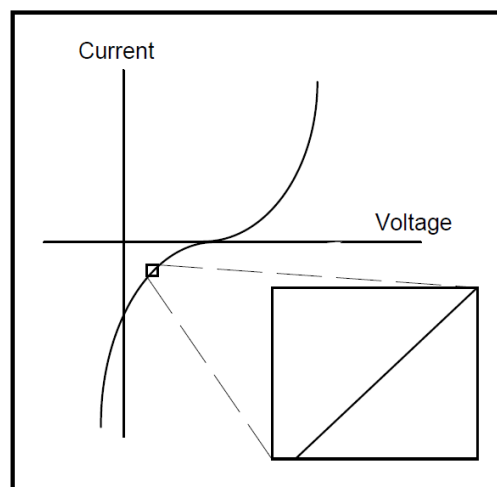


Figure 11: Current versus Voltage Curve showing Pseudo-Linearity

Steady State Systems

Measuring an EIS spectrum takes time (often many hours). The system being measured must be at a steady state throughout the time required to measure the EIS spectrum. A common cause of problems in EIS measurements and their analysis is caused by a drift in the system during the measurement process.

In practice a steady state can be difficult to achieve. The cell can change through adsorption of solution impurities, growth of an oxide layer, buildup of reaction products in solution, coating degradation, temperature changes, to list just a few factors (GAMRY-TUT-1, 2015).

4.2.5 Gauge factor

Gauge factor (GF) is a quantity that expresses the fractional change in electrical resistance (FCR) compared to strain. A high gauge factor expresses that the cementitious is sensitive because the relative change resistivity is large compared to the strain, and the opposite for a small gauge factor. The gauge factor is calculated by the following equation:

$$Gauge\ Factor = \frac{\Delta R/R_0}{\Delta L/L_0} = \frac{FCR}{\varepsilon}$$

Where R_0 is the initial electrical resistance and ΔR is the change in resistance.

Since the gauge factor is influenced by different experimental procedures, the cementitious bulk resistivity, moisture, curing time, w/c ratio, fiber volume fraction, etc. this factor should only be considered as a rough indicator of sensitivity, and cannot be used to compared sensitivity of functional filler without considering other internal and external factors.

4.2.6 Fundamentals of Potentiostat – EIS- Measurement techniques

The following subchapter describes the test set-up used to measure the impedance of steel fiber reinforced concrete (SFRC) as well as the decision-making process to find the best input parameters for the EIS-Software for the used experimental method (GAMRY-APN-2, 2015).

Overview of 2-, 3-, and 4 electrode Measurements & Applications

For a better understanding of the chosen experimental mode (2-, 3-, or 4- probe method) and input parameters a short introduction of electrochemical measurements according to the used GAMRY Interface 1000 (see Figure 12) is given.



Figure 12: GAMRY Interface 1000 Potentiostat/Galvanostat/ZRA

Electrochemical experiments range from simple potentiostatic (chronoamperometry), to cyclic voltammetry (Potentiodynamic) to complex AC techniques such as impedance spectroscopy. Moreover, each individual technique may have multiple possible experimental setups. The following discusses the aspect of different setups and electrodes -or probes- possible to use.

The GAMRY potentiostat is a 4-probe instrument which means there are four relevant leads that need to be placed in any given experiment. The two leads – Working (green) and Counter (red) - carry the current and the other two – Working sense (blue) and Reference (white) are sense leads which measure voltage (potential). The GAMRY instrument can be setup to run 2-electrode, 3-electrode, or 4 electrode measurements. Therefore, it is important to understand why and how to use the different modes.

Electrodes

An electrode is a (semi-)conductive solid that interfaces with an electrolyte (solution). The **Working electrode (green)** is the designation for the electrode being studied. In corrosion experiment it is the material that is corroding, in physical electrochemistry experiments, this is most often an inert material which passes current to other species without being affected by that current. The **Counter or Auxiliary electrodes (red)**, is the electrode in the cell that completes the current path. All electrochemistry experiments (with non-zero current) must have a working-counter pair. In most experiments, the Counter is the current source/sink and thus inert materials are ideal but not necessary. **Reference electrodes (white)** are electrodes that serve as experimental reference points so they are a reference for the potential (sense) measurement. The reference electrode should therefore hold a constant potential during testing, ideally on an absolute scale. This is accomplished by having a little or no current flow through them by being “well-poised” which means that even if some current does flow it does not affect the potential. Commonly used electrodes for this purpose are: silver/silver chloride, saturated calomel, mercury/mercury oxide, mercur-

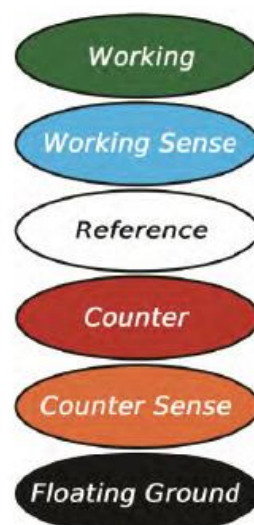


Figure 13: GAMRY color-codes leads

ry/mercury sulfate, copper/copper sulfate and normal hydrogen electrodes. Also, any conductive material can be used as a reference electrode but if potential measurements are to be reported that need to be compared with other systems, use of a non-standard reference requires additional experimentation and explanation.

Two-Electrode Experiment

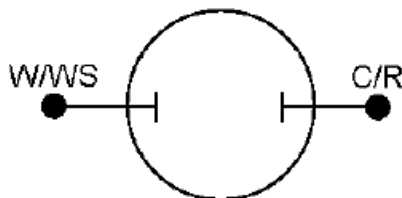


Figure 14: Two-electrode cell setup

- Measurement:
 - Measures the Voltage drop across the whole cell
- General Cases/Usage:
 - Measurement of the whole cell Voltage is significant (e.g. batteries, fuel cells, super-capacitors)
 - Counter electrode potential can be expected to be constant during the experiments (general in systems with very low currents or short time experiments)

The Two-Electrode Method is the simplest cell setup but often have far more complex results and corresponding analysis. In the two-electrode setup the current-carrying electrodes are also used for sensing measurement by connecting the Working (W) and Working Sense (WS) together. Figure 14 shows a diagram of a 2-electrode cell setup where Working (W) and Working Sense (WS) are connected to a (working) electrode and Reference (R) and Counter (C) are connected to a second (aux, counter, or quasi/pseudo-reference) electrode. The Counter Sense (CS) does not have any task in this setup. This setup measures the whole cell and thus measures the complete voltage dropped by the current across the electrochemical cell. If a map of the whole cell potential matches Figure 15, than the Working Sense lead is at Point A and the Reference lead is at point E, This configuration measures the voltage drop across the whole cell.

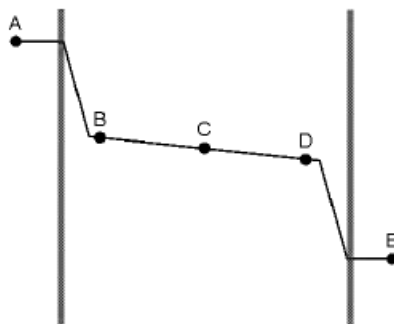


Figure 15: Measured (sample) potential map across a whole cell

Working lead is at point A and Counter lead is at point E

Three-Electrode Experiment

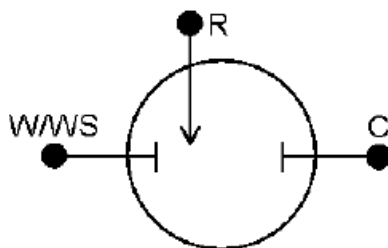


Figure 16: Three-Electrode Cell setup

- Measurement:
 - Measures one half of cell and thus the potential change of the working electrode
 - The measurement is independent of any changes occurs at counter electrode
- General Cases/Usage:
 - Allows a specific reaction studied with confidence and accuracy.
 - This is the most common setup used in electrochemical experimentation

In the Three-Electrode Method the Reference lead is separated from the Counter and connected to a third electrode (see Figure 16). This electrode is often positioned close to the working electrode – which has both Working and Working Sense leads attached. Again, the Counter Sense (CS) does not have any task in this setup. This electrode setup has a distinct experimental advantage over the two-electrode setup: It measures only a half of the cell which is the potential changes of the working electrode. The measurement is independent of changes that may occur at the counter electrode.

Four-Electrode Experiment

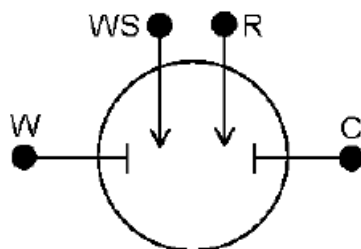


Figure 17: Four-Electrode Cell setup

- Measurement:
 - Measures the impedance between the Working Sense and Reference electrode
 - Potential of any electrochemical reaction occurring at Working and Counter electrode is not measured.
- General Cases/Usage:
 - Allows the measurement of impedance across some solution-phase interface such as membrane or liquid-liquid junction.
 - This setup can be used to make very accurate measures of solution resistance or
 - Measures of resistance across the surface of some materials (Solid-state cells)

In the Four-Electrode Method all four electrodes are separated as illustrated in Figure 17. This setup measures the potential between the Working Sens and Reference electrode which can be referred to a measurement between point B-D in Figure 15. In this mode, the potential for any electrochemical reaction occurring at the working and counter electrode are not measured. What is being measured is the effect of an applied current on the solution itself or some barrier in the solution. Hence, the Four-Electrode Method is the most appropriate setup for impedance measurement of concrete beams. (GAMRY-APN-1, 2015).

Potentiostat fundamentals

A potentiostat controls the voltage difference between a working electrode and a reference electrode. Both electrodes are contained in an electrochemical cell. The Potentiostat implements this control by injecting current into a cell through a counter or auxiliary electrode. In almost all applications, the potentiostat measures the current flow between the working and counter electrodes. The controlled variable is the cell potential and the measured variable is the cell current. A potentiostat requires an electrochemical cell with three electrodes.

Working electrode is the electrode where the potential is controlled and the current measured. In many experiments this electrode is an inert material such as gold, platinum or glassy carbon. In these cases, the working electrode serves as an area where the electrochemical reaction takes place. For corrosion test this electrode is a sample of the corroding metal. (For batteries, the potentiostat is directly connected to the anode or cathode).

Reference electrode is used to measure the working electrode potential. This electrode should have a constant electrochemical potential if current flows through it. The most common lab reference electrodes are the saturated calomel electrode (SCE) and the silver/silver chloride (Ag/AgCl) electrode. In field probes, a pseudo-reference (e.g. a piece of the working electrode material) can be used.

Counter electrode or auxiliary electrode is a conductor that completes the cell circuit. In lab cells, it is an inert conductor of platinum or graphite. In field probes it generally is another piece of the working electrode material. The current that flows into the solution via the counter electrode leaves the solution via the working electrode.

The electrodes are immersed in an electrolyte/solution and the collection of the electrodes, the solution, and the container holding the solution are referred to as an electrochemical cell.

Simplified Schematic of a Potentiostat

A simplified schematic of a GAMRY Instruments Potentiostat is sketched in Figure 18. In this schematic, **x1** on an amplifier indicates that the amplifier is an unity-gain differential amplifier. The output voltage of this circuit is the difference between its two inputs. The blocks labeled **Voltage** and **Current x R_m** are the voltage and current signals that are sent to the system A/D converters for digitization.

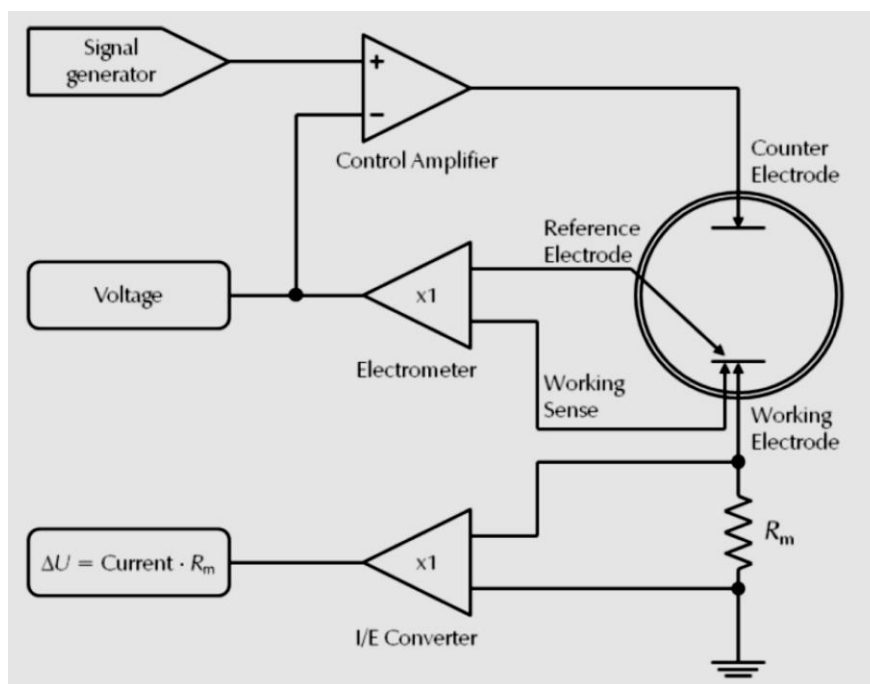


Figure 18: Simplified schematic of a potentiostat [2]

The Electrometer circuit measures the voltage difference between the reference and working electrodes. Its output has two major functions: it is the feedback signal in the potentiostat circuit, and it is the signal that is measured whenever the cell voltage is needed. An ideal electrometer has zero input current and an infinite input impedance. Current flow through the reference electrode can change its potential. In practice, all modern electrometers have input currents close enough to zero so that this effect becomes negligible.

The current to voltage (**I/E Converter**) measures the cell current. It forces the cell current to flow through a current measurement resistor R_m where the voltage drop across R_m is measured and equal to the cell current. If the cell current changes over a wide range of magnitude a number of different resistors R_m are needed to measure the current precisely e.g.: Measurement of small currents requires larger R_m values and vice versa. Therefore an I/E auto ranging algorithm is often used to select the appropriate resistor values (GAMRY-APN-3, 2015).

The Control Amplifier is a servo amplifier which compares the measured cell voltage with the desired voltage and drives current into the cell to force the voltages to be the same. Note that the measured voltage is input into the negative input of the control amplifier. A positive perturbation in the measured voltage creates a negative control amplifier output. This negative output counteracts the initial perturbation and is known as negative feedback.

The Signal circuit is a computer controlled voltage source. It is generally the output of a Digital-to-Analog (D/A) converter that converts computer-generated numbers into voltages. A proper choice of number sequences allows the computer to generate constant voltages, voltage ramps and even sine waves at the signal circuit's output. When a D/A converter is used to generate a waveform such as a sine wave or ramp, the waveform is a digital approx. of the equivalent analog waveform, with small voltage steps. The size of the steps is controlled by the resolution of the D/A converter and the rate at which it is being updated with new numbers.

4.3 Types of electrodes

For the measurement of electrical resistance several different types of electrodes are investigated by researchers. However, according to (Han, Yu, et al., 2014), the electrode material should have low electrical resistance and a stable conductivity.

Electrodes for piezoresistive measurements can be divided into two categories: Embedded- and surface electrodes. Furthermore, the material of the electrodes is also an important factor that influences the measurement results. One of the most common electrode material used for electrical resistance measurement is copper or stainless steel. Copper tape or wire can be used as surface electrodes, and copper mesh, plate or wire is used as embedded electrodes that can be arranged in the mold either before the casting or in the fresh mortar after the casting. For surface electrodes, it is recommended to combine the copper tape or wire with a conductive liquid, such as paint or epoxy, which reduces potential air voids between the surface of the specimen and the conductive tape. The conductive liquid can either be silver paint, silver epoxy, copper paint, etc.

4.3.1 Embedded electrodes

Embedded electrodes can be categorized into plate -, mesh - and wire electrodes. Figure 19 illustrates how mesh electrodes can be arranged in a customized mold.

(Han et al., 2006) found that the compressive strength of cube specimen is depended on the mesh size, while, the electrical resistivity is independent of mesh size. Han et al. results indicated that the compressive strength is reduced with a mesh size of $1.66 \times 1.66 \text{ mm}^2$ due to reduced bonding, but the compressive strength was not influenced by mesh electrodes with the size of $2.03 \times 2.03 \text{ mm}^2$ and $2.56 \times 2.56 \text{ mm}^2$.

Furthermore, these results should only be considered as indications because of the small number of specimens tested, and further research is recommended within this field.



Figure 19: Copper mesh pre-arranged in a customized mold (Teomete, 2014)

4.3.2 Surface electrodes

Surface electrodes can be used to either measure the surface resistance, the diagonal volume resistance and longitudinal volume resistance. The type of resistance measured depends on the electrodes position relatively to each other. For instance, the surface resistance can be measured by placing all electrode on the same side (Figure 20-A). The volume resistance can be measured by

placing the line electrodes diagonally to each other (Figure 20-B), and loop electrodes can be used for measuring the longitudinal volume resistance (Figure 20-C).

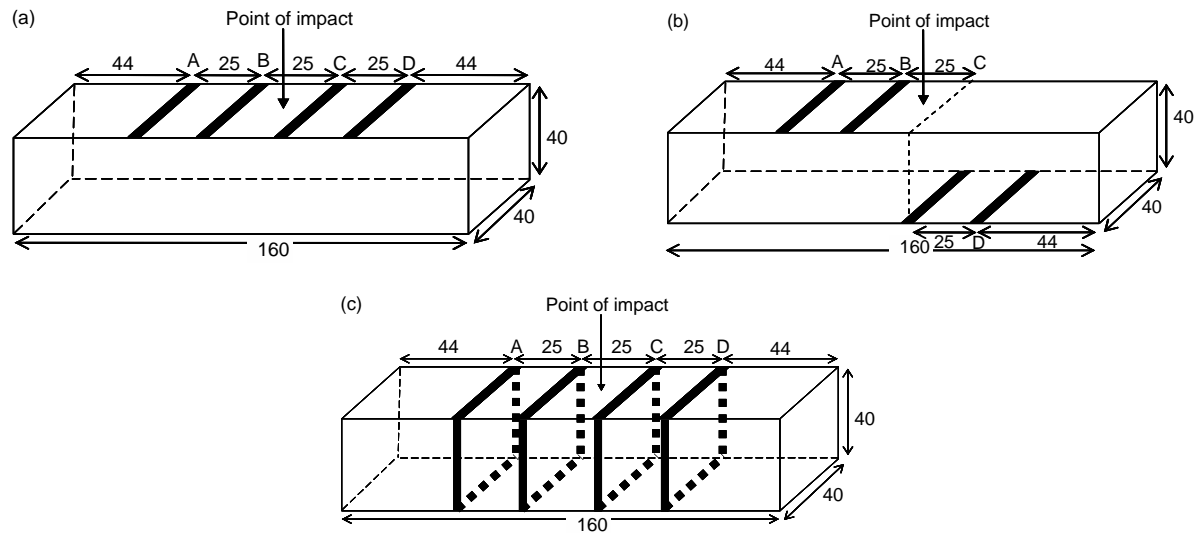


Figure 20: Surface electrodes in different positions (Meehan, Wang, & Chung, 2010)

(Chiarello & Zinno, 2004) analyzed the resistance and standard deviation for different configurations of electrode setups (Figure 21) on concrete mixtures with carbon fibers serves as functional fillers. The electrical measurements were conducted by an alternating current (AC) with a frequency of 100 kHz. The results indicate that the four-probe method with embedded electrodes (S3) had the lowest resistance and standard deviation (Table 4).

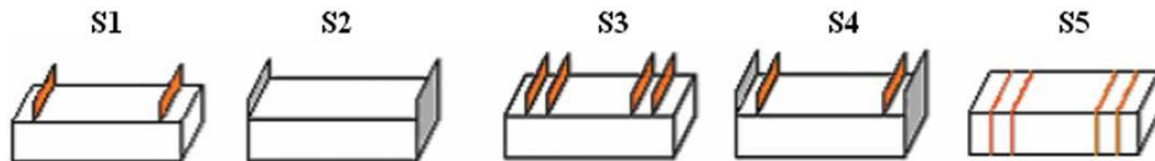


Figure 21: Two- and four-probe electrical configurations (Chiarello & Zinno, 2004)

Table 4 –Electrical resistance for various configurations (Chiarello & Zinno, 2004)

	\bar{R} (Ω)	sd (Ω)	CV (%)
S1	230.5	51.4	22.3
S2	91.5	11.3	12.4
S3	37.1	2.5	6.70
S4	54.8	3.8	6.90
S5	80.9	61.6	76.0

4.4 Influence of additives and curing properties

4.4.1 Hydration time

The experimental study of (Chiarello & Zinno, 2004) illustrated the change in electrical conductivity during the hydration process for different volume fraction of carbon fibers.

(Chiarello & Zinno, 2004) concluded that the low volume fraction of 0.075 (Figure 22-1) was more dependent on the ionic conductivity of the electrolyte (free/pore water). While, the volume fraction of 0.45 (2) and 1.6 (3), had a conductive network that was more dominated by the electronic conductivity provided by the functional filler. In addition, this type of experiment can also be used to determine the threshold value of fiber volume fraction where the sensitivity is less dependent of the ionic conduction.

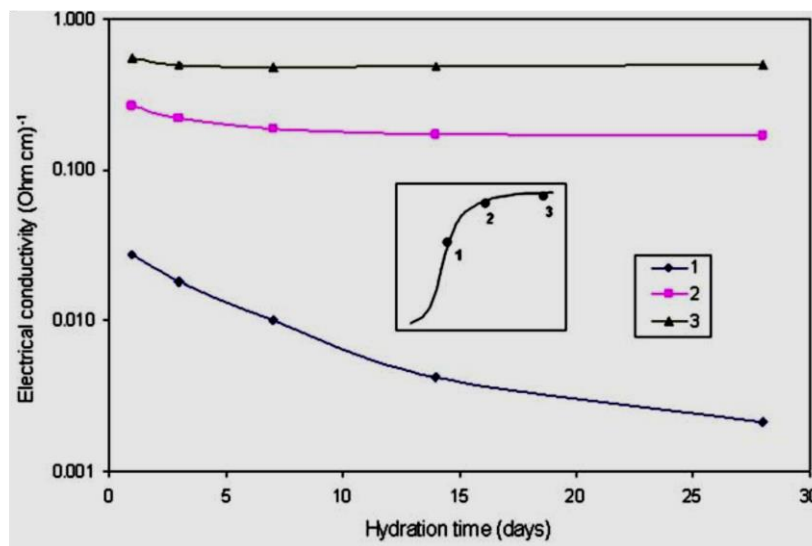


Figure 22: Electrical Conductivity & Hydration time (Chiarello & Zinno, 2004)

Volume fraction: 1-0.075/2-0.45/3-1.6

As expected, the electrical conductivity depends on the hydration time for low fiber content, but the degree of conductivity reduction is related to the amount of functional fillers and the type of electrical conductivity. During hydration process, the amount of free water is reduced which explains the increase of electrical resistivity – and decrease of conductivity - with the hydration time due to reduced ionic conduction.

4.4.2 Temperature

In a study carried out by (Azhari, 2008), the electrical resistivity in carbon fiber reinforced concrete were found to be highly influenced by changes in the temperature. The electrical resistivity was measured in environmental chambers with both high (20 °C to 60°C) and low (-15°C to -30°C) temperature ranges. Figure 23 and Figure 24 present the change in electrical resistivity for high- and low-temperature ranges, respectively. The electrical resistivity decreased with higher temperature and increased with lower temperature for both temperature ranges. For the high range tempera-

ture, the resistivity increased/decreased with a rate of 35 ohm-cm/°C, and for the low-temperature range, the resistivity increased/decreased with a rate of 22 ohm-cm/°C.

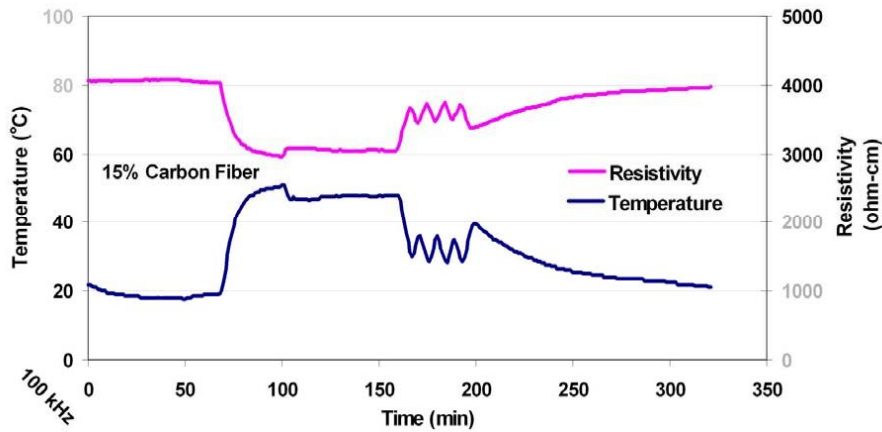


Figure 23: High-Temperature Range (20°C to 60°C) (Azhari, 2008)

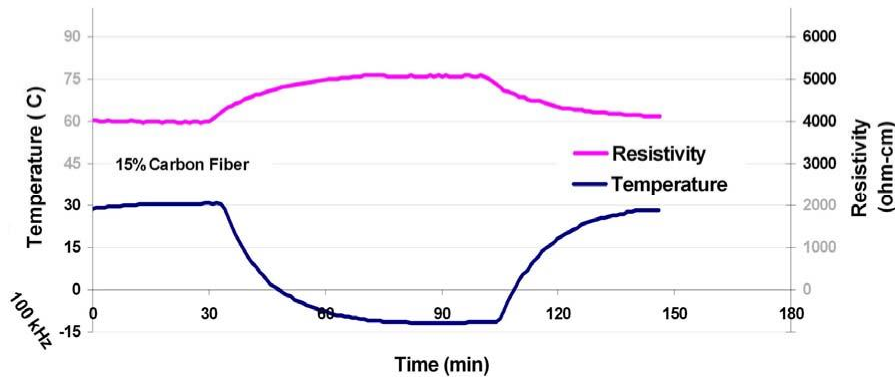


Figure 24: Low-Temperature Range (-15°C to -30°C) (Azhari, 2008)

4.4.3 Sand/cement ratio

(Chiarello & Zinno, 2004) investigated the influence of sand-cement ratio and its conductivity. The experiments were conducted on specimens with carbon fiber content of 0.5 vol. %, fiber length of 3 mm, and water/cement ratio of 0.45. The different sand/cement-ratios were as following: 0, 0.5, 1.0, 1.5, 2.0, 2.5, and 3.0. All specimens were tested after one day and 28 days of curing. Figure 25 illustrates how the conductivity decrease with increasing sand-cement ratio and curing time.

Increasing sand amount act as an insulator and cut the electron flow between the carbon fibers and electrolyte (evaporable water).

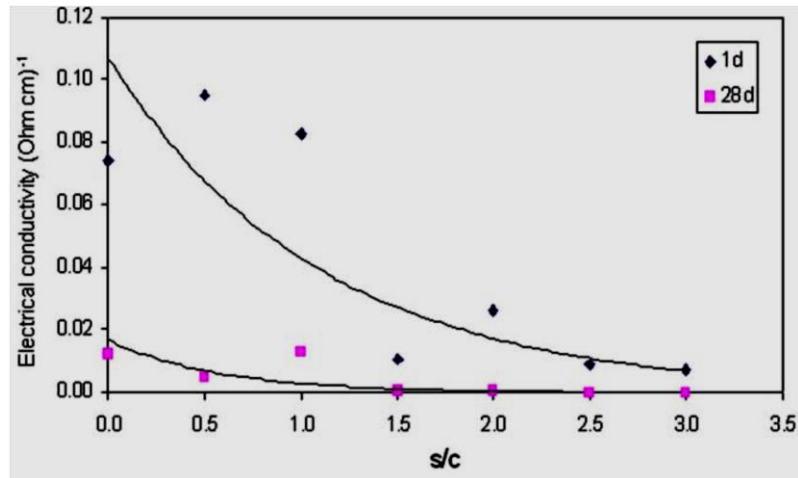


Figure 25 : Effect of S/C ratio on the conductivity after 1 day and 28 days of curing (Chiarello & Zinno, 2004).

4.4.4 Gravel/sand ratio

(Baeza, Chung, Zornoza, Andi3n, & Garc3s, 2010) investigated the influence of different gravel/sand ratios and carbon fibers contents on the resistivity after 28 days of curing. The carbon fiber length was 3.5 mm and diameter of 7.2 μm . The water/cement ratio was 0.50, and the sand/cement ratio was 0.75. The sand/cement ratio of 0.75 is within the conductive range of (Chiarello & Zinno, 2004) presented work.

The different gravel/sand ratios were as following: 0.15, 0.25, 0.375, 0.75, 1.50, 2.00, 2.50, and 3.00. The contents of carbon fibers (% mass of cement) were: 0.75, 1.00, 1.50, 1.75, and 2.00. Their results indicated an rapidly increase of resistivity at gravel/sand ratio of 2.0 and for carbon fibers content below 1.50 % mass of cement (Figure 26) (Baeza et al., 2010).

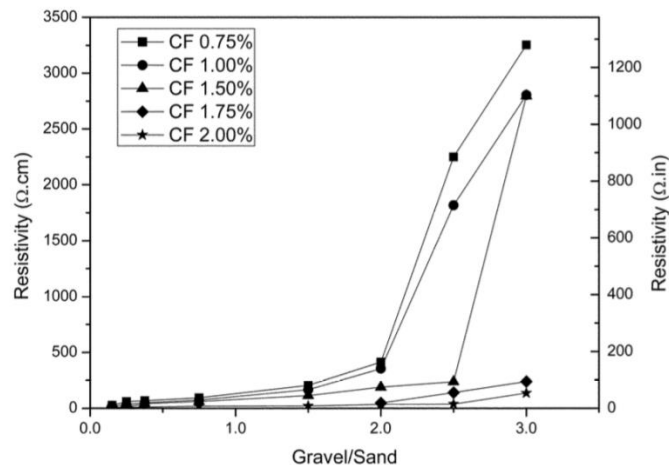


Figure 26: Gravel/sand ratio and Carbon Fiber content (% mass of cement) effect on resistivity (Baeza et al., 2010)

4.5 Functional fillers

Functional fillers are used to increase conductivity and provide self-sensing properties in concrete mixtures. This section will present different functional fillers with emphasis on electrical resistivity and their capability to create self-sensing properties.

4.5.1 Steel

Steel fibers

(Solgaard et al., 2013) compared the change of electrical resistivity due to different steel fiber volume fraction. The steel fiber length was 35 mm with a diameter of 0.55 mm. The mortar mix composition is presented in Table 5 Table 5 –Mortar mix compositions (Solgaard et al., 2013). The electrical resistance was measured by an alternating current with a frequency of 126 Hz. Results of this study showed a reduction of electrical resistivity with increasing steel fiber volume (.

Table 4 Concrete compositions for Series A (assuming s.s.d. conditions of aggregates and 1 vol.% air)

Materials	Quantity (kg/m ³)			
	Plain concrete	SFRC		
	0.0 vol.%	0.5 vol.%	1.0 vol.%	1.5 vol.%
Cement	500	500	500	500
Water	240	240	240	240
Sand (0–4 mm)	1,563	1,550	1,536	1,523
Steel fibres	0	39	78	117

Table 5 –Mortar mix compositions (Solgaard et al., 2013)

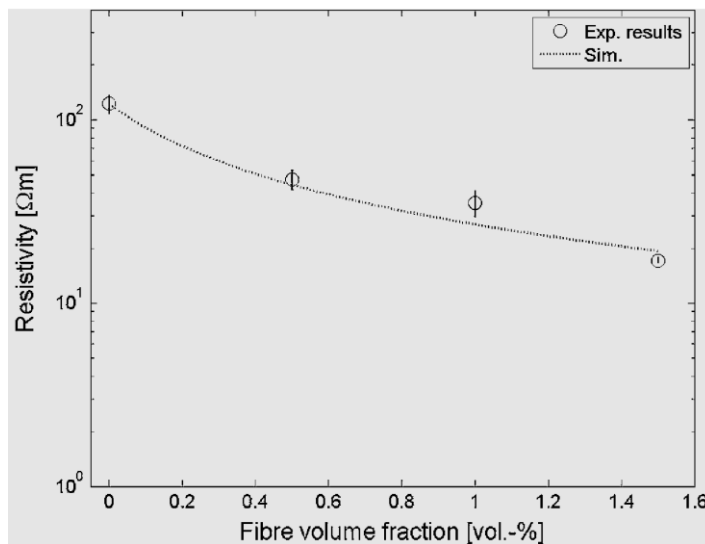


Figure 27: Resistivity change due to fiber volume fraction (Solgaard et al., 2013)

Steel micro-fiber

(Teomete, 2014) investigated the self-sensing ability of cementitious materials with brass coated steel fibers with a length of 6 mm, diameter of 290 μm and volume fraction of 1%. The results indicated a strong linear relationship between the change in electrical resistance, compressive strain, and tensile strain.

(Banthia, Djeridane, & Pigeon, 1992) compared the electrical resistance of carbon and steel micro-fiber. The steel micro-fiber length was 3 mm and diameter of 25 μm , and carbon micro-fiber length was 6 mm and diameter of 18 μm . The results indicated that carbon fibers have a greater effect on improvement of conductivity compared to steel. This is explained by the high specific surface area of carbon fiber which creates a better inter-fiber continuity. The carbon fibers used in this experiment had a much greater specific surface area of 134 000 mm^2/g compared to the steel fiber with a specific surface area less than 20 382 mm^2/g . While, the steel micro-fibers used in the experiment were much more conductive themselves compared to carbon micro-fiber. This indicates that the specific surface area of fibers is more important than the electrical conductivity of fiber materials. (Banthia et al., 1992).

(Wen & Chung, 2003) did a comparative study of cementitious composites with stainless steel – and carbon fibers. The stainless steel fiber length was 6 mm and diameter of 8 μm , carbon fiber length was 5 mm with a diameter of 15 μm . Several cement mixtures were prepared with different fiber content. The fiber volume fractions were as following: 0.36 Vol% steel fibers, 0.72 Vol% steel fibers, and 0.5 Vol% of carbon fiber. The results indicated that the resistivity was more noisy for the specimens with steel fibers compared to carbon fibers. The specimens containing steel fiber of 0.36 Vol% had a higher reversible change in resistivity compared to 0.72 Vol % steel fiber. While, the highest reversible change resistivity was found for the specimens with carbon fibers. Based on the observations of noise and reversibility of the electrical resistance, (Wen & Chung, 2003) concluded that carbon fibers are more suitable for piezoresistive strain measurement.

4.5.2 Carbon

Carbon fibers

The comparative experiments presented earlier in the paper concluded that carbon fibers are more suitable than micro-steel fiber for achieving a self-sensing concrete. (Yeh, Chang, & Liao, 2015) conducted several experiments with low carbon fiber content concrete with only 0.2 Vol. %, fiber length of 15 mm and diameter of 7 μm . The experiment investigated the sensitivity for specimens subjected to uniaxial compression, uniaxial tension, three-point bending, and a large-scale RC portal push-over frame. Results from the experiments demonstrated that low carbon fiber content of 0.2 Vol % is sufficient for strain and damage measurement for all the different loading conditions.

It is important to note that the carbon fiber content of 0.2 Vol % is only sufficient for providing better piezoresistive properties to the cementitious composites, while this fiber volume content is considered as too low for any mechanical performance enhancement.

(Wen & Chung, 2006) investigated steel reinforcing bars and their influence to surface resistance for a cementitious composite with carbon fibers. A fiber content of 0.48 vol %, fiber length of 5 mm,

and diameter of 15 μm were chosen. Results of flexural bending test on beam specimens indicated that steel reinforced rebar increases the change in fractural resistance. More specific, the change in fractural surface resistance increased 70% on the compression side and 40 % on the tension side. These results can also be compared with numerical analysis of current density distribution conducted by Zhu and Chung (2007). Figure 28 illustrates the current density analysis for cementitious with carbon fiber compared to the distance from the top surface on a specimen cross section of 4x4 cm^2 .

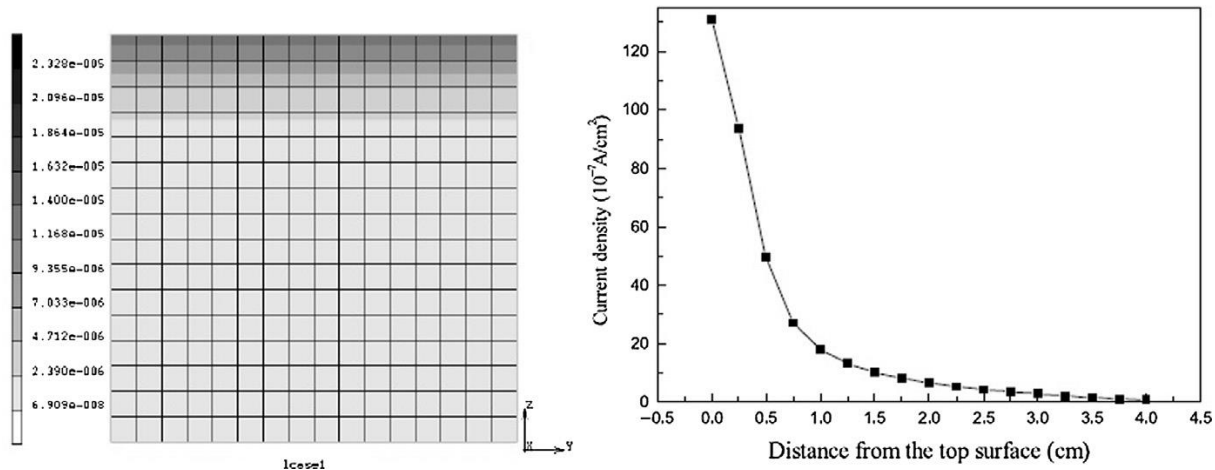


Figure 28: Numerical analysis of current density distribution for line electrode (Zhu & Chung, 2007)

(Chen, Wu, & Yao, 2004) analyzed how the electrical conductivity change with different volume fraction of carbon fibers. Their results indicated that the change in electrical conductivity plateau off at a fiber volume fraction of 0.8%. Figure 29 presents the electrical conductivity for various fiber volume fraction of carbon fiber.

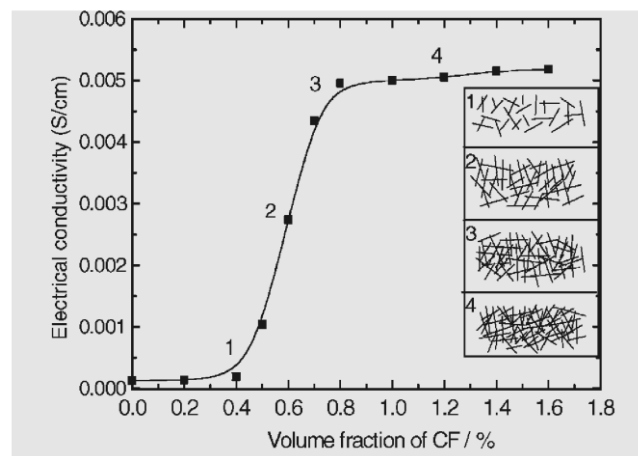


Figure 29: Relationship between conductivity and volume fraction of carbon fibers (Chen et al., 2004)

4.5.3 Carbon Nano Tubes

Carbon Nano Tubes (CNT) are nanocomposites which improves mechanical properties and also provides piezoresistive properties to concrete mixtures (Konsta-Gdouts & Aza, 2014). CNT can be specified into two groups: Single-Wall Carbon Nano Tubes (SWCNT) and Multi-Wall Carbon Nano Tubes (MWCNT) where SWCNT are formed by only one tube layer of a hexagonal carbon flake sheet, and MWCNT contain of multiply tube layers (Konsta-Gdouts & Aza, 2014). Figure 30 and Figure 31 show the SWCNT (A) and MWCNT (B) and there bond in cementitious materials.

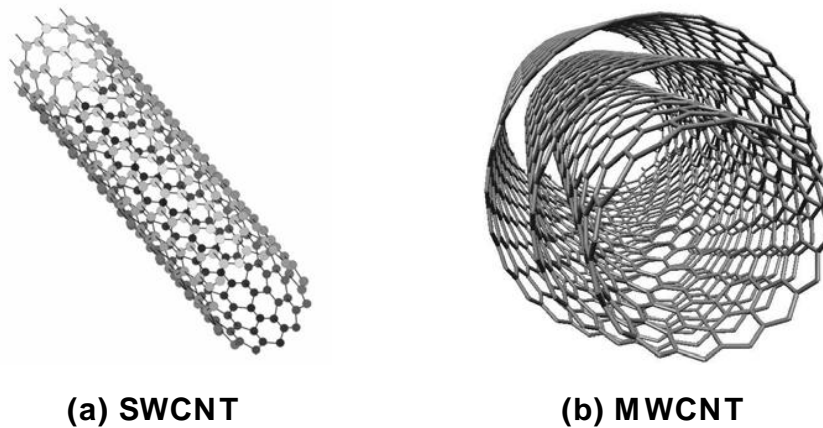


Figure 30: Single and Multi Carbon Nano Tubes SWCNT and MWCNT

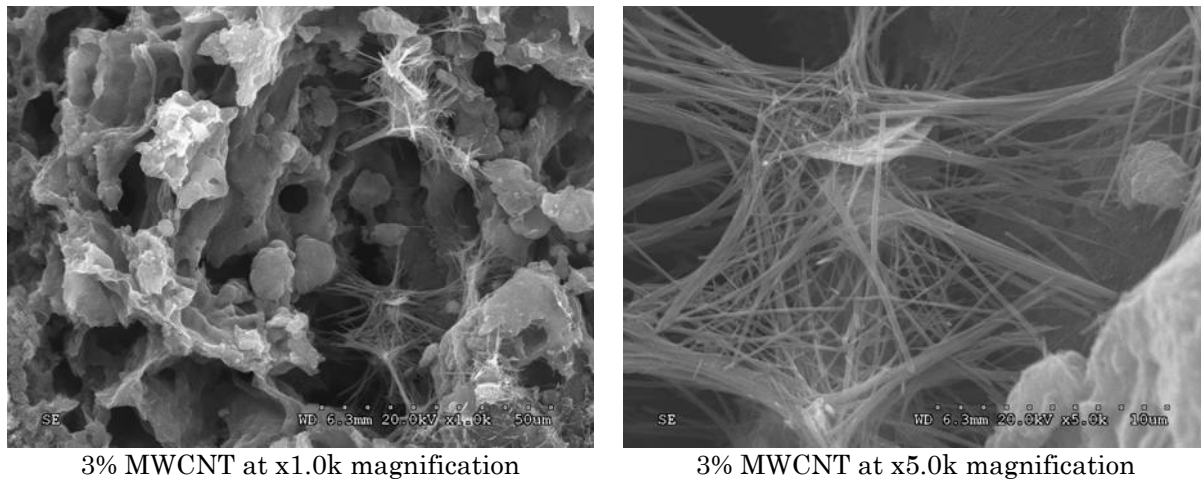


Figure 31: SEM pictures of 3% MWCNT (Azhari, 2008)

(Konsta-Gdouts & Aza, 2014) experimented with real-time damage assessment by using MWCNT as the functional filler. The experiment investigated piezoresistive properties on cementitious composites containing 0.1 wt% and 0.3 wt% of cement of MWCNT with an water-cement ratio of 0.3. The MWCNT specifications were as following: tube diameters of 20-40 nm and lengths in the range of 10-100 μm . A sonicator was used to disperse the MWCNT in water before adding cement. A real-time damage assessment was conducted by applying a cyclic load to the beam specimen. The results indicated the highest average change in resistivity for the composition with MWCNT 0.1 wt%.

4.5.4 Graphene

Graphene Oxide (GO) leads to increased compressive and flexural strength of concrete mixtures. (Liu, Xu, Yu, Gao, & Tong, 2016) compared the mechanical and piezoresistive properties of cementitious materials containing graphene nano-platelets (GNPs) and graphene oxide nano-platelets (GONPs). The GNPs content of a 6.4% ratio of cement weight had great influence on the electrical conductivity. The sensitivity was accurate for both natural-dried and oven dried conditions for the specimen. While the GONPs had the same electrical resistance as the control specimen without GO's which concluded they have no piezoresistive effect.

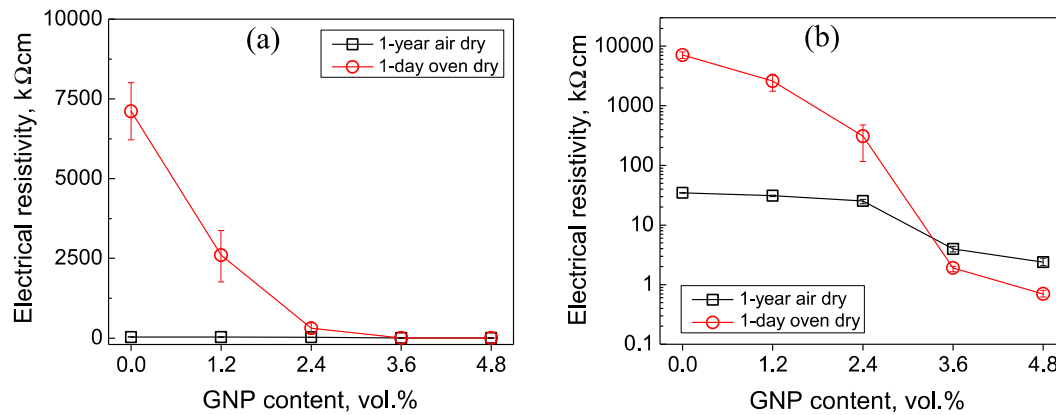


Figure 32: Electrical resistivity for different GNP vol. % (Le, Du, & Pang, 2014)

4.5.5 Overview of self-sensing research

Reference	Functional Filler	V _f - vol. %	Method	Hz	Gauge Factor	GF	Resistivity
(Teomete, 2014)	Steel microfiber: Steel fiber coated with brass	1%	Four-probe 15V DC	NA	Compression Split tensile test	42-193	Resistivity not given
(Banthia et al., 1992)	Microfiber: Steel (S) and Carbon (C) Hybrid-Fiber composites (S&C)	S- 1%, 3%, 5% C- 1%, 3%, 5% C-1.5% & S-1.5% C-1.0% & S-2.0% C-2.0% & S-1.0%	AC Videobridge Low current: 0.1mA Imped. Spectra. Fig.3	7500 Hz See Fig. 3	Resistivity	NA	See Table 3 28 days, plain matrix: 66 - 117 Ohm-cm 28 days, steel fiber: 7439- 31 921 Ohm-cm 28 days, Carbon fiber: 78- 820 Ohm-cm
(Wen & Chung, 2003)	Microfiber: Stainless steel & Carbon	<u>Steel fibers (S):</u> 0.36% & 0.72% <u>Carbon fibers (C):</u> 0.5%	Four-probe DC Current: S- 0.36 % - 9.2mA S-0.72% - 0.98mA C - 0.5% - 89 μA	NA	Tensile Compression test	Tensile: 90-4560 Comp.: 200-350 (less variance with carbon fibers) See Table 1	See Table 1 S-0.36%:16 Ohm-cm S-0.72%:57 Ohm-cm C-0.5%: 1.5x10 ⁴ Ohm-cm (Large variance can be explained by different applied currents)

Reference	Functional Filler	V_f - vol. %	Method	Hz	Test	Gauge Factor	Resistivity
(Solgaard et al., 2013)	Steel fiber: L=35 mm, Ø=0.55 mm	0.0%, 0.5%, 1.0%, 1.5%	Two-probe Plate electrodes AC	126 Hz	Resistivity	NA	See Fig. 3 Resistivity decreased with an in- creasing V_f .
(Wen & Chung, 2006)	Carbon fiber	0.48%	Four-probe DC	NA	Bending w/o steel rebar	See Table 1 for FCR at deflections	Resistivity not given
(Yeh et al., 2015)	Carbon fiber	0.2 %	Four-probe DC	NA	Compression (C) Tensile (T) Cyclic bend- ing(B) Large scale (L)	(C1) 187.1 - 253 (C2) 20.9 - 24.9 (T) 9.5 - 19.5 Highest GF: (B-comp.side) 1031 (B-tens. side) 844	Resistivity not given
(Hou & Lynch, 2005)	<u>ECC</u> Carbon fiber Steel fiber	<u>ECC</u> 1) 2% PVA fibers &0.4% Carbon fiber 2) 2% PVA fibers & 0.1% steel fibers	Two-probe DC (5V) AC (-5V to 5V)	<u>AC</u> 5 Hz	Tensile test Cyclic test Large scale cycli- cally loaded bridge piers	<u>DC - Tensile test</u> <u>ECC</u> 100 <u>ECC+Carbon</u> 21 <u>ECC + Steel</u> 18	<u>DC ECC</u> 2.5×10^6 Ohm-cm <u>ECC+Carbon</u> 0.8×10^6 Ohm-cm <u>ECC + Steel</u> 1.9×10^6 Ohm-cm
(Liu et al., 2016)	Graphene: GNOPs GNPs	1.6 % of c.w. 3.2 % of c.w. 6.4 % of c.w. 12.8 % of c.w.	DC DC applied 300 sec. ahead of testing due to polarization ef- fect	NA	Cyclic compres- sive loading	NA	See table 5 and 6 Varies with % of c.w. content and condition

References of Table:

- Banthia, N., Djeridane, S., & Pigeon, M. (1992). Electrical resistivity of carbon and steel micro-fiber reinforced cements *Cement and Concrete research - Pergamon Press Ltd*, 22, 804-814.
- Han, B., Ding, S., & Yu, X. (2014). Intrinsic self-sensing concrete and structures: A review. *Measurement*, 59, 18.
- Hou, T.-C., & Lynch, J. P. (2005). Conductivity-based strain monitoring and damage characterization of fiber reinforced cementitious structural components. *Proceedings of SPIE 12th Annual International Symposium on Smart Structures and Materials, San Diego, CA, March 6-10, 2005*.
- Liu, Q., Xu, Q., Yu, Q., Gao, R., & Tong, T. (2016). Experimental investigation on mechanical and piezoresistive properties of cementitious materials containing graphene and graphene oxide nanoplatelets. *Construction and Building Materials*.
- Solgaard, A. O. S., Geiker, M., Edvardsen, C., & Kuter, A. (2013). Observations on the electrical resistivity of steel fibre reinforced concrete. *Materials and Structures*, 47, 15.
- Teomete, E. (2014). Transverse strain sensitivity of steel fiber reinforced cement composites tested by compression and split tensile tests. *Construction and Building Materials*.
- Wen, S., & Chung, D. D. L. (2003). A comparative study of steel- and carbon-fibre cement as piezoresistive strain sensors. *Advances in Cement Research*.
- Wen, S., & Chung, D. D. L. (2006). Self-sensing of flexural damage and strain in carbon fiber reinforced cement and effect of embedded steel reinforcing bars. *Carbon*, 44, 1496–1502.
- Yeh, F.-Y., Chang, K.-C., & Liao, W.-C. (2015). Experimental Investigation of Self-Sensing Carbon Fiber Reinforced Cementitious Composite for Strain Measurement of an RC Portal Frame. *International Journal of Distributed Sensor Networks*, 2015.

5 Experimental method

5.1 Material properties

For the four-point bending test an approx. one year old Hybrid Fiber Reinforced Concrete (HyFRC) beam with dimension of 6 x 6 x 24 in³ was used to evaluate the correlation of deflection and impedance during loading. The concrete specimen was immersed in water for eight days and dried in laboratory environment at ambient temperature over 24 days prior testing. Details of the concrete mixture are listed in Table 6.

Table 6: Concrete mixture for self-sensing measurement

Composite	Cement (kg)	Aggregates (kg)		Water (kg)	V _f (% , based on total composite volume)		
		Coarse	Fine		PVA	Steel (30 mm)	Steel (60 mm)
HyFRC	423	775	853	228	0.2	0.5	0.8

5.2 Test specification

A four-point bending test was conducted with purpose of evaluate the correlation between the change in electrical resistance and deflection during loading. A copper tape with dimensions of 0.8 x 6 in (20 x 152 mm) was glued to the specimen with silver conductive epoxy to serve as electrodes and ensure appropriate conductivity. An overview of the specimen and the positioning of the electrodes are shown in Figure 33 and Figure 34. Due to the setup applied, the resistance measurement takes place on the surface of the specimen and a few mm in depth as recognized in Figure 28 on. Hence, the surface of interest was chosen to be the tension zone during bending. A general overview of the bending test setup and the positioned specimen/electrodes can be seen in Figure 35 and Figure 36. During bending test force and mid-span displacement was recorded as well as the impedance at a frequency of 100 kHz and an amplitude of ± 10 mV with a GAMRY Potentiostat device.

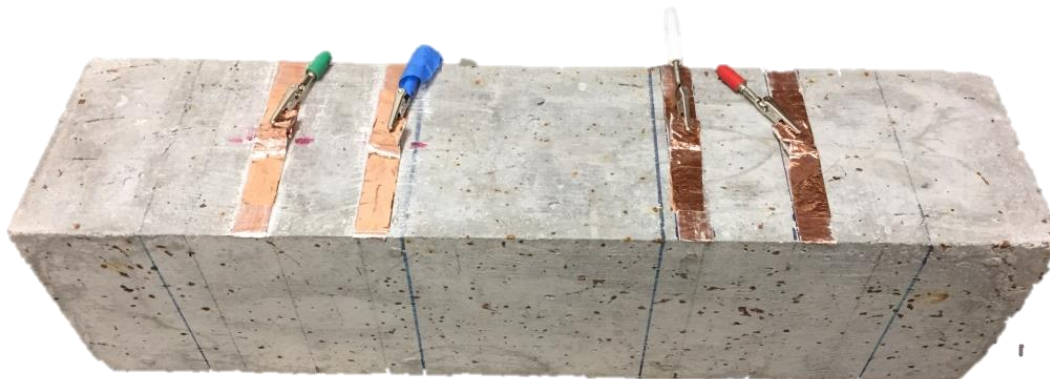


Figure 33: Overview Copper Electrodes

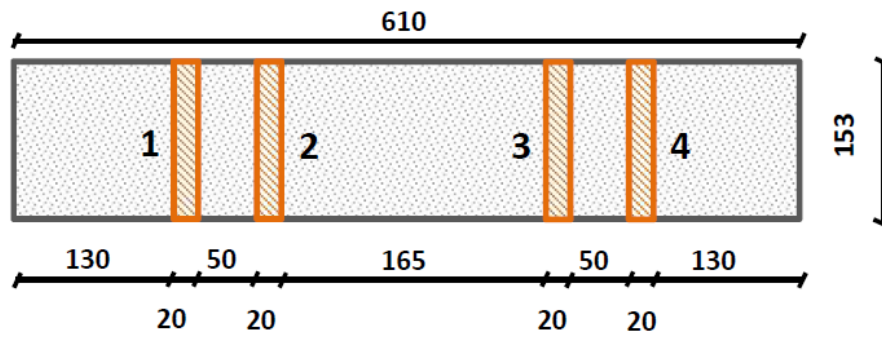


Figure 34: Positioning of Electrodes



Figure 35: Bending Test Setup



Figure 36: Overview of impedance measurement configuration

6 Results

6.1 Stability pre-test

To ensure stable electrical condition during testing and to eliminate polarization effects, a long-term stability test was conducted over 105 min before conducting the bending test. The parameters were kept to the same as for the bending test with a frequency of 100 kHz of and an amplitude of ± 10 mV. Figure 37 shows the impedance over Time for the Real-(Z-real) and Imaginary-(Z-imag) part as well as the complex impedance (Z-mod) in Ohm.

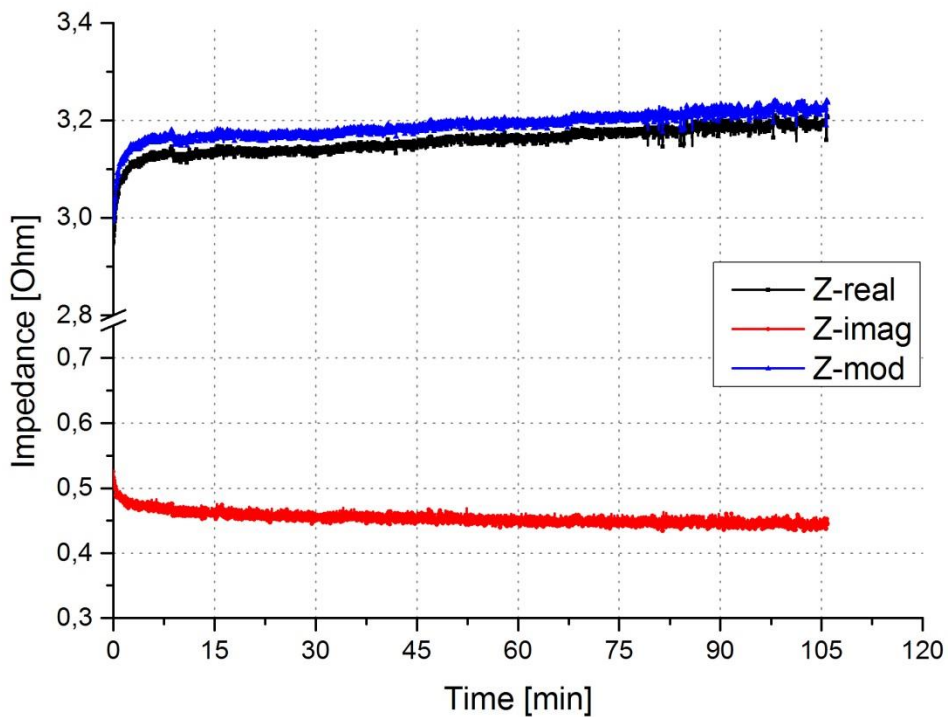


Figure 37: Long-term stability impedance test

The percentage change of impedance is shown in Figure 38. The real- and complex impedance changes in the first 7 min up to 6% of its initial value. For the following 90 minutes the impedance increases linearly to 8 %. After the stabilization time of 7 minutes the change of Impedance per 15 min is approx. 0.5 %. The duration of the bending test took 20 minutes. therefore an accurate stabilization is given after 7 min. This stabilization time was considered before starting the bending test and will be explained in more detail in Figure 40 and Figure 41.

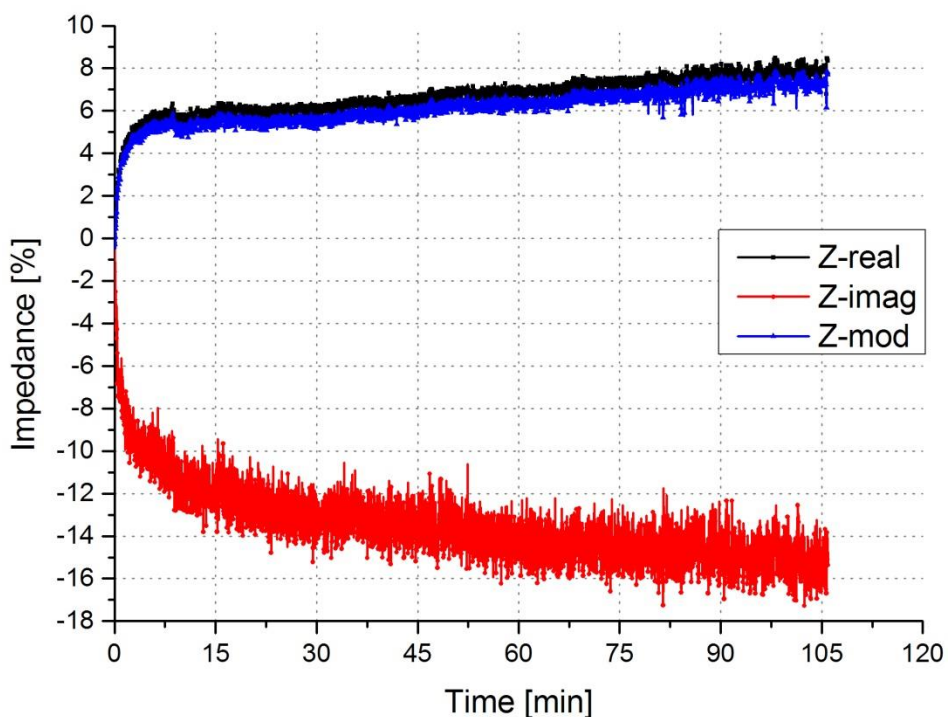


Figure 38: Long-term Stability impedance test -percentage change

The strong relation between imaginary part and phase-angle as well as between real and complex impedance results from the mathematical background of complex impedance calculation. The relation between real-, imaginary-, and complex impedance is given by:

$$Z - real = z - mod \cdot \cos(\varphi)$$

and

$$Z - imag = z - mod \cdot \sin(\varphi)$$

where φ is the phase-angle shown in Figure 39. Due to the low phase-angle the real and complex impedance almost overlay in Figure 38. Therefore, the imaginary impedance results are small with a corresponding evolution as for the phase-angle.

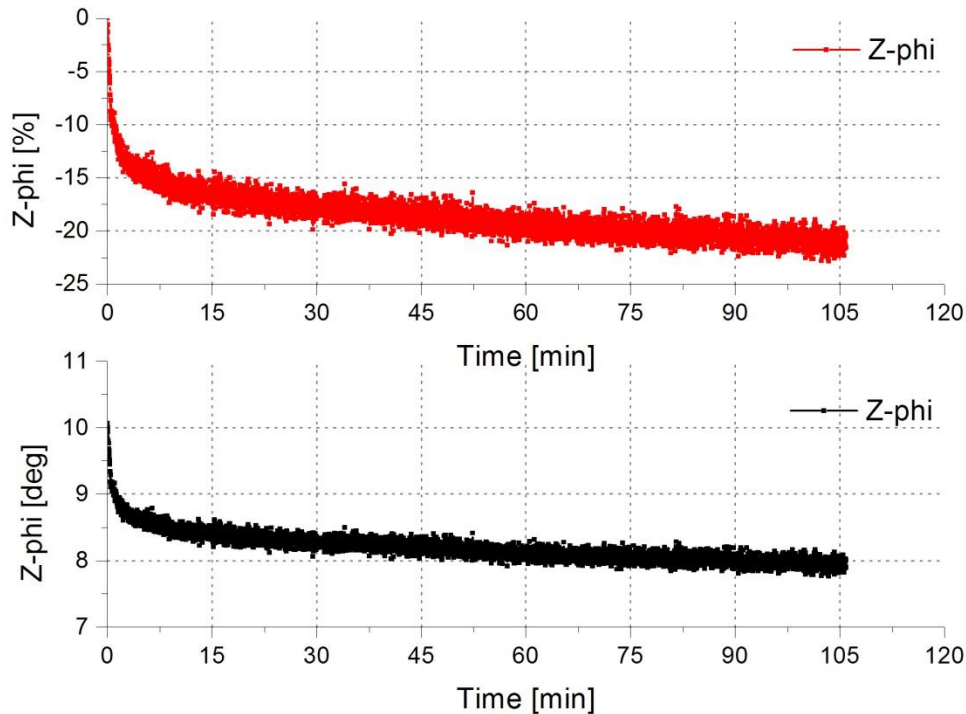


Figure 39: Long-term Stability impedance test – phase angle

6.2 Stability measurement before bending test

After arranging all the measurement devices and preparations for the four-point bending test, the specimen was preloaded with 0.1 kips to achieve force closure. The pre-stabilization test results, presented in subchapter 3.1, indicated that 7.5 minutes was sufficient for achieving electrical stability in the system. Based on this result, the impedance measurement was started 7.5 min ahead of the bending test. The change in impedance- and force over time is shown in Figure 40, and the percent change can be seen in Figure 41. The force increased by 2% during the stabilization test. Real-, and complex impedance are overlying in Figure 40 and Figure 41, therefore only the complex and imaginary impedance can be seen. Two changes of 5 % in impedance were observed at 2 and 6 minutes before the bending test. The first change at 2 minutes can be explained by a possible electrical interference during testing (the 5% change took place over 30 sec. and corresponds to 11 measurement points), hence the second change can be interpreted from a same effect. Nevertheless, it should be noted that both data, impedance measurement, and bending test were recorded with dif-

ferent computer systems, and therefore a time offset occurred. During data processing, the time offset of approximately one minute could be detected and corrected by an immense change of almost 90 % in impedance during the first crack propagation. The initial crack and stiffness decrease is highlighted with a gray region in both Figure 40 and Figure 41.

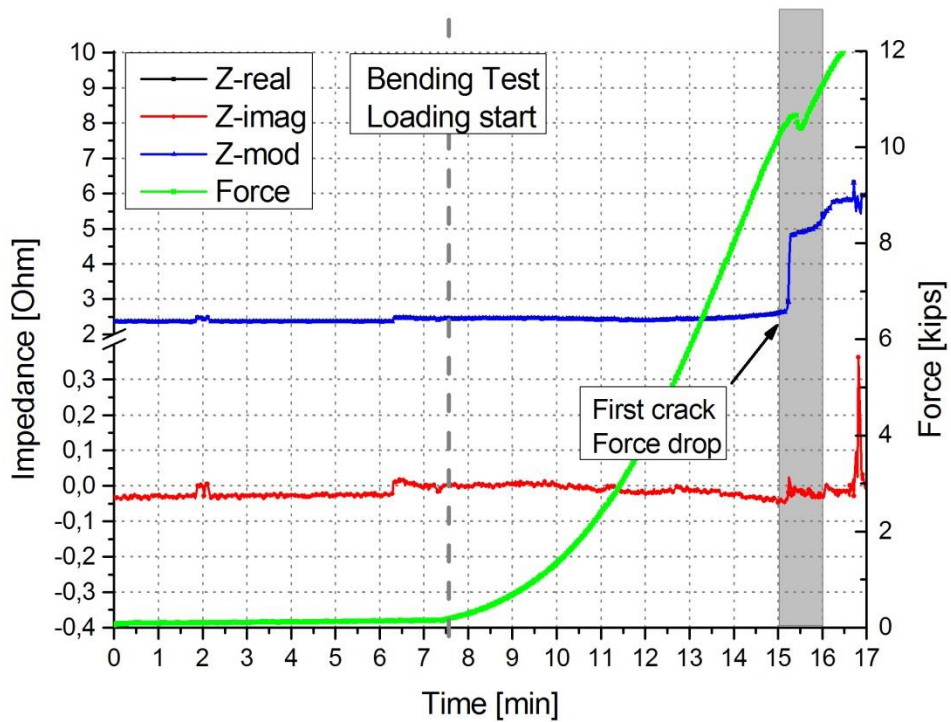


Figure 40: Stability before bending test – impedance-force

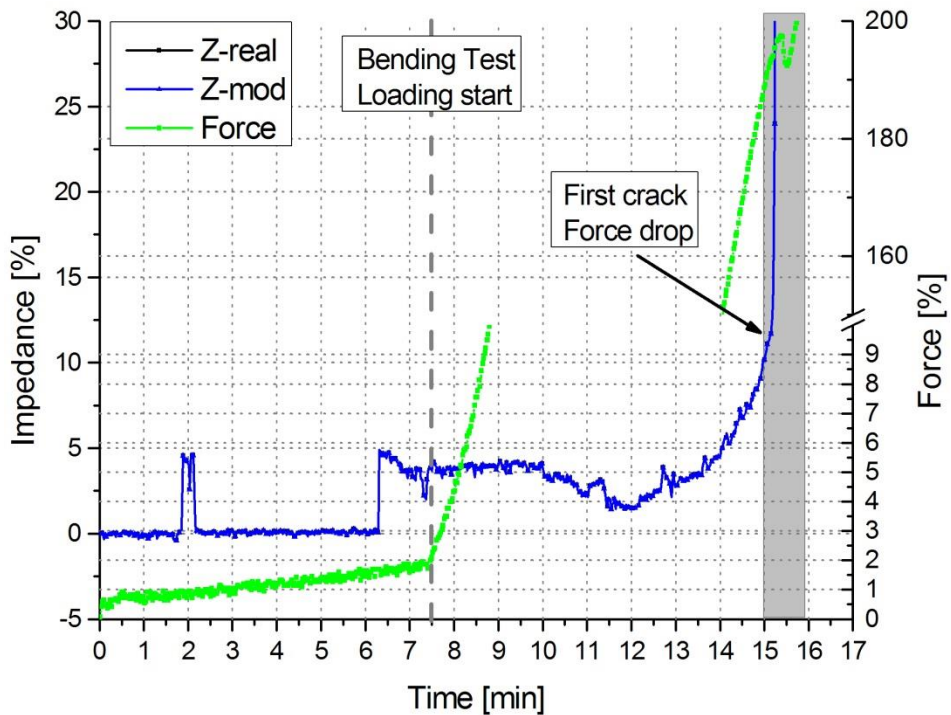


Figure 41: Stability before bending test – impedance

6.3 Bending test and Impedance measurement

After electrical stability was reached the bending test was conducted with an overall displacement rate of 0.016 in/min (0.04 mm/min). Figure 42 shows the displacement rate in 2.5 minutes interval during testing time. Loading of specimen started at 7.5 minutes and the test was stopped at 30 minutes after an overall displacement of 0.24 in (6.1 mm).

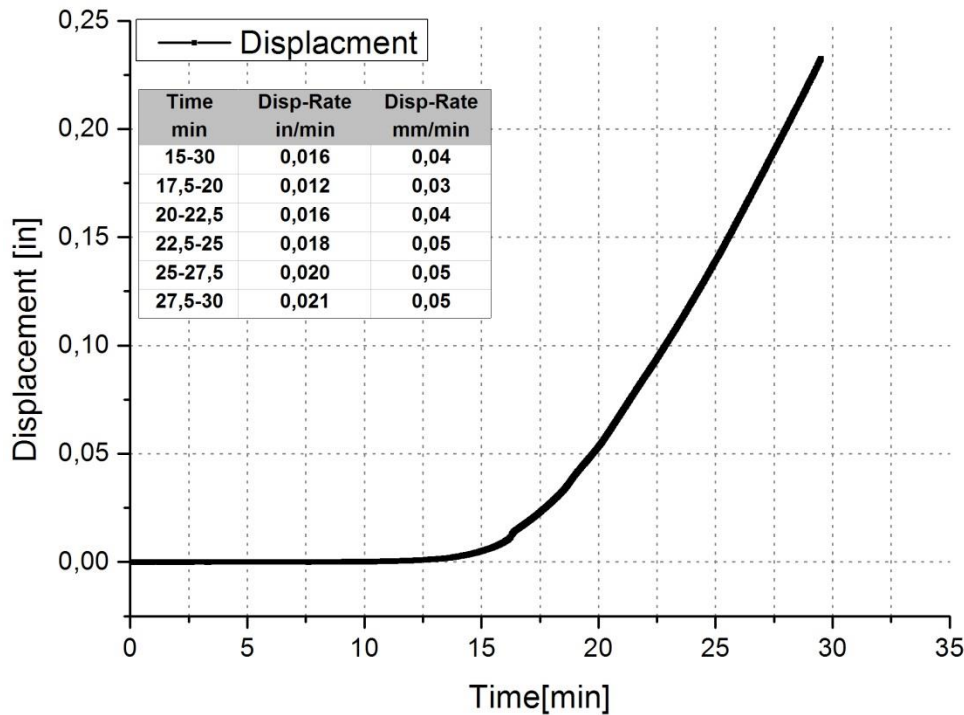


Figure 42: Displacement Rate during bending test

Figure 43 presents the change of complex impedance and applied force over time. Loading started at 7.5 minutes and increased to 10.5 kips at 15 minutes until the first crack/stiffness decrease occurred. This leads to an abrupt rise in impedance from their initial value of 2.6 to 4.9 Ohm. This is followed by a constant increase of impedance during loading until the test was stopped at 30 min and 0.24 in displacement.

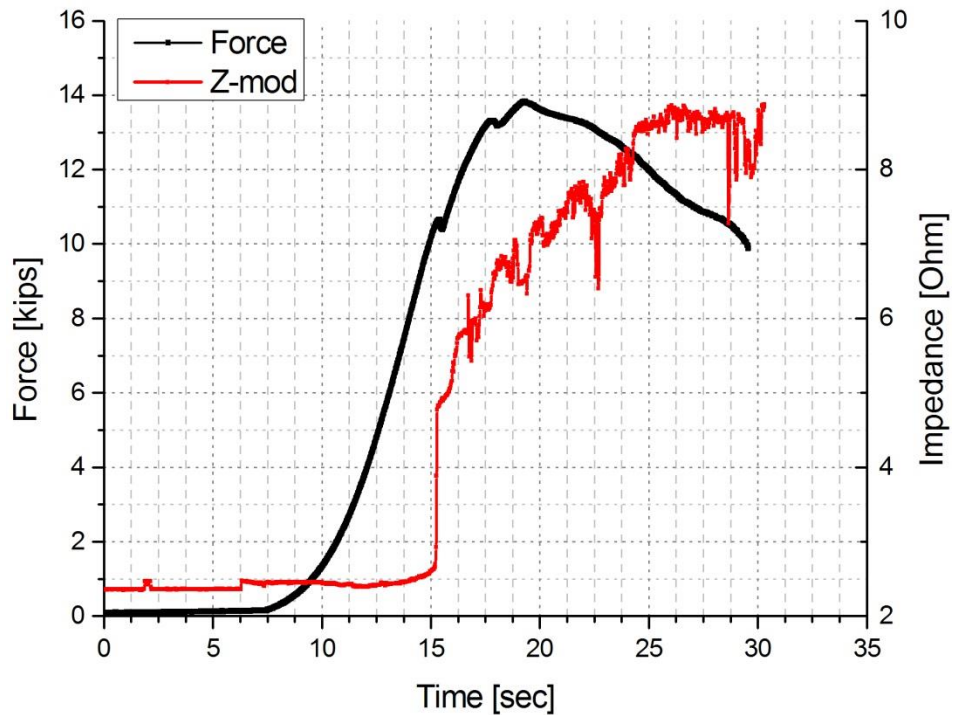


Figure 43: Bending Test Time – Z-mode

In Figure 44 and Figure 47, both impedance and force over displacement are plotted. These Figures show the increase of impedance during elastic zone up to a displacement of 0.01 in (0.25mm) from 2.4 to 2.6 Ohm followed by an abrupt increase, caused by the first stiffness drop, of impedance from 2.6 to 4.9 Ohm.

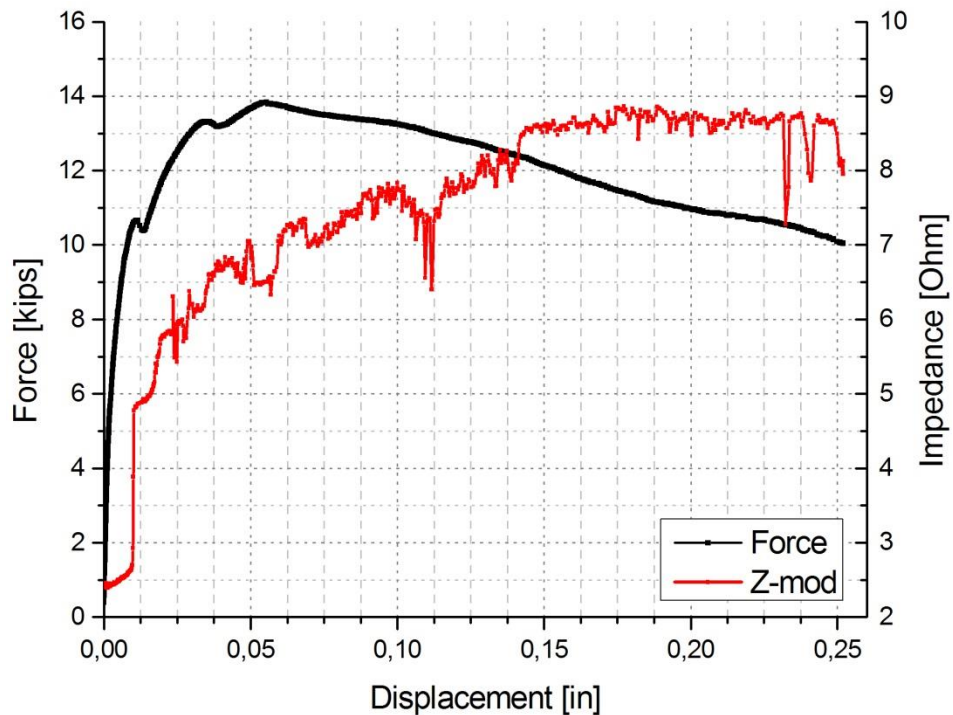


Figure 44: Bending Test Displacement – Z-mode

The fractural change of impedance ΔR , which is given by

$$\Delta R = \frac{R - R_0}{R_0}$$

where R is the instant impedance and R_0 the initial impedance is shown in Figure 45 and Figure 46. A change of 12 % within elastic zone and a prompt increase of 90% at the first crack initiation can be detected. This is followed by a continuous increase of impedance until 270 % or 8.7 Ohm. Considering the imaginary impedance and the phase-angle in Figure 48 and Figure 49 a correlation between strain-softening the stiffness decrease over displacement and reduction of imaginary impedance and phase-angle can be observed.

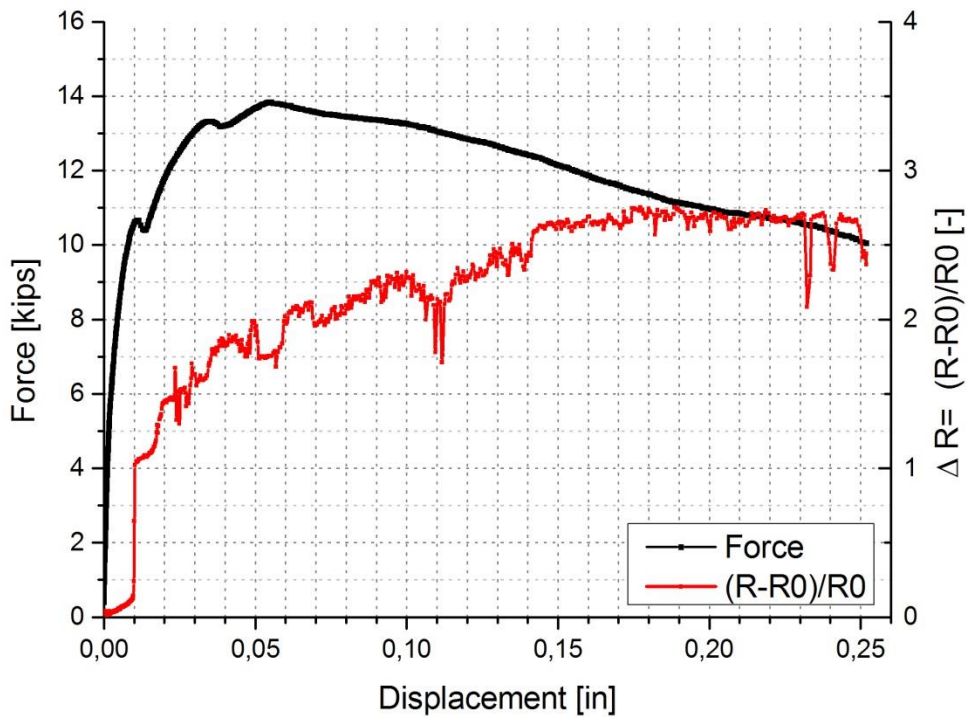


Figure 45: Bending Test Displacement Delta R

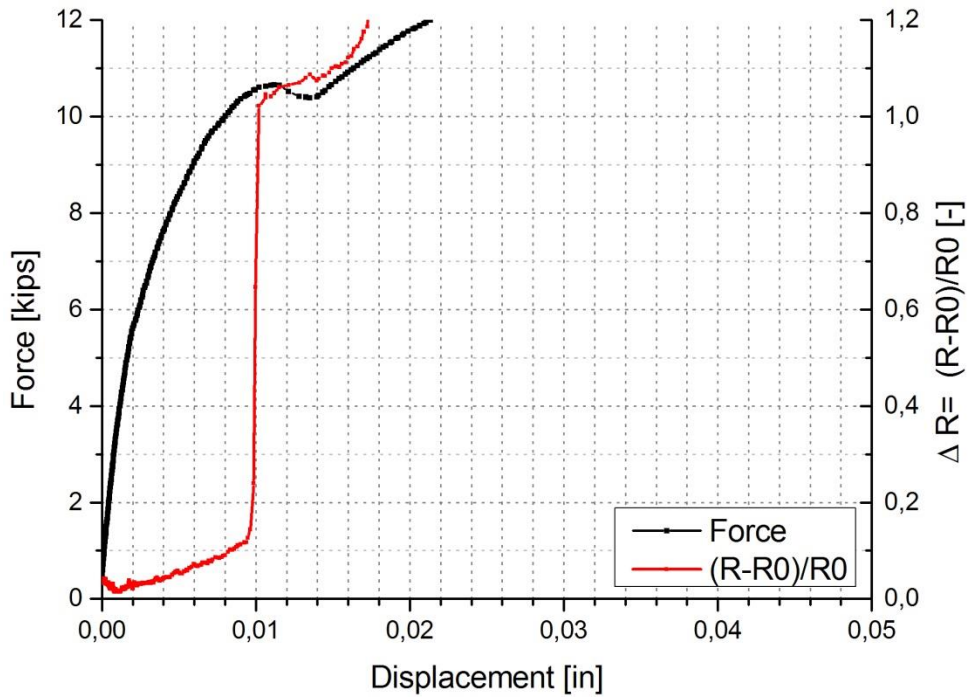


Figure 46: Bending Test Displacement Delta R - Zoom

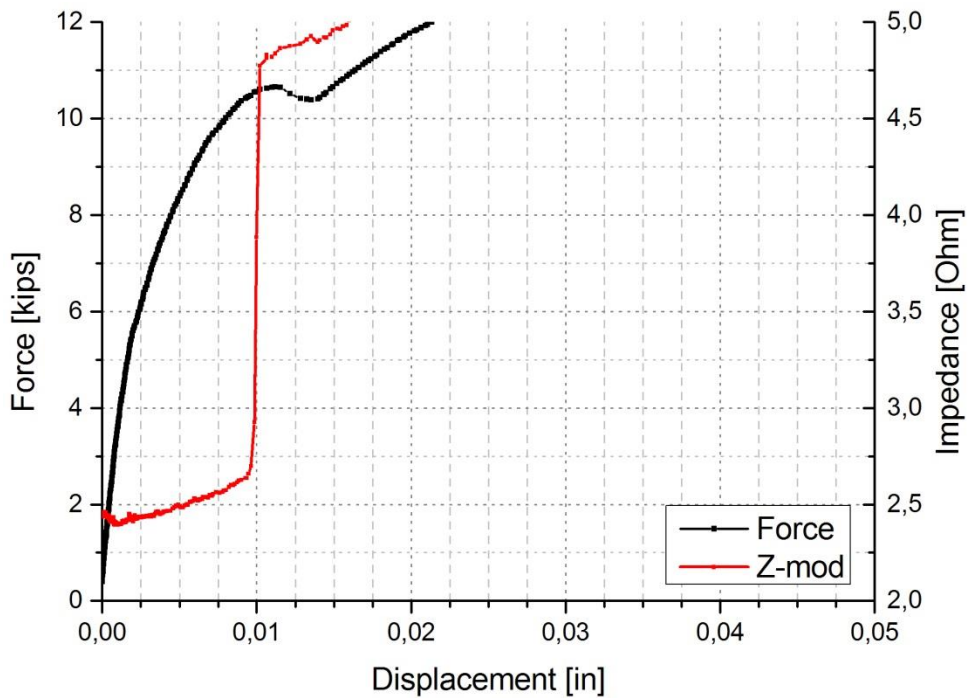


Figure 47: Bending Test Displacement Z-mode- Zoom

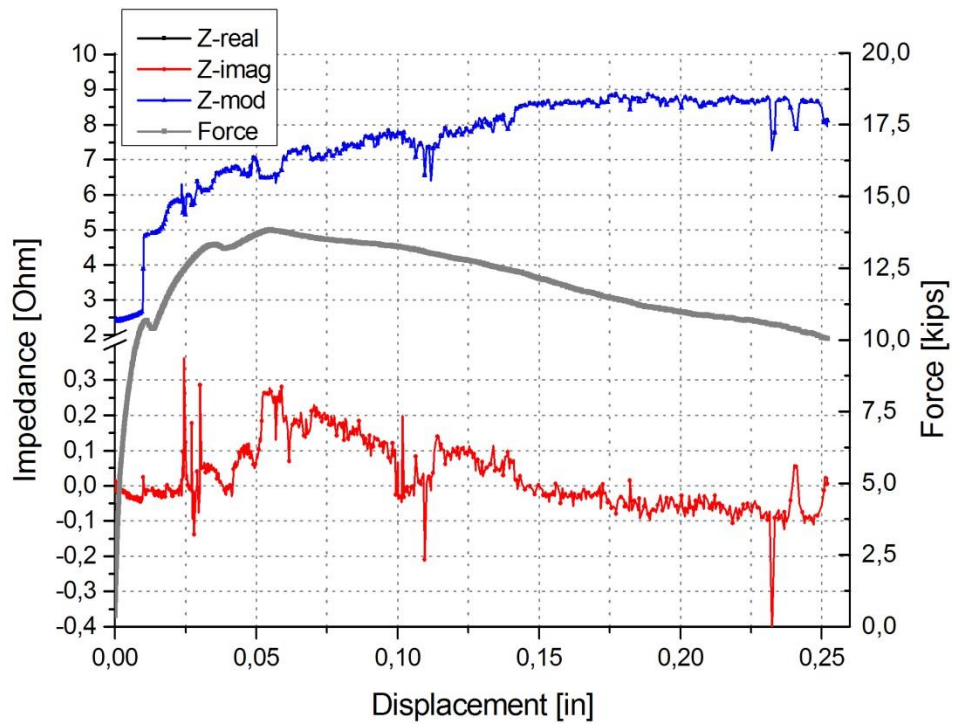


Figure 48: Bending Test Displacement-Z-Disp

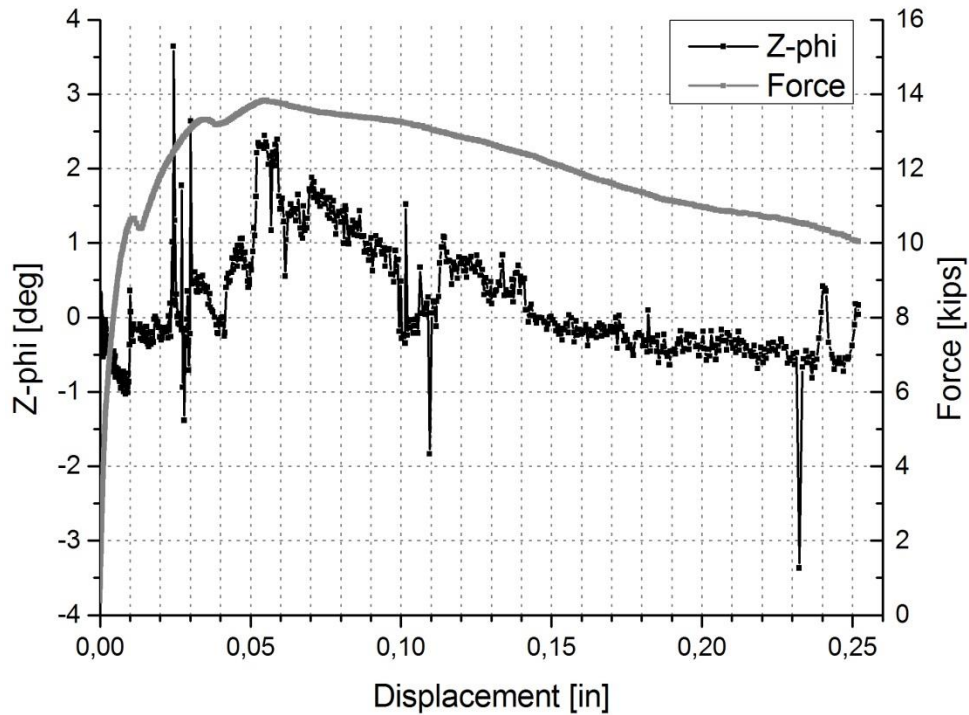


Figure 49: Bending Test Displacement-Z-Phi

7 Conclusion

A four-point bending test on a 6 x 6 x 24 in³ beam specimen was conducted to evaluate the ability to detect a correlation between stress stage and change in impedance of Steel Fiber-Reinforced Concrete. The test specimen was immersed in water for eight days and dried in laboratory environment at ambient temperature for 24 days prior testing. During bending test the applied force, resultant displacement and impedance at the tension zone was recorded. The results show a good correlation between the change in impedance and stress stage during bending test. For instance, an increase of tensile stress during elastic stage could be detected by an increase of impedance as well as a decrease of stiffness during initial crack propagation leads to a change of approx. 90 % in Impedance. At this point it should be noted that the impedance was measured with a potentiostat at 100 kHz frequency and ± 10 mV amplitude. Furthermore, the specimen is assumed to be partly-saturated during testing which leads to a conductive pore solution. So the measured impedance can not only be credited to the conductivity of steel fibers. Rather it is the sum of conductive pore solution and steel fibers. Nevertheless, correlation between deflection and impedance measurement with a commercially available potentiostat is identifiable but further research on the influence of moisture content and conductivity of pore solution is suggested. This results show the ability of the developed HyFRC mixture to serve as self-sensing material for structural health monitoring.

8 Acknowledgement

The authors gratefully acknowledge financial support by the Austrian Marshall Plan Foundation in Vienna which enabled this research project at the University of California, Berkeley, USA.

9 References

- Azhari, F. (2008). *Cement-Based Sensors For Structural Health Monitoring*. (Master of applied science), The University of British Columbia (Vancouver), Vancouver
- Baeza, F. J., Chung, D. D. L., Zornoza, E., Andión, L. G., & Garcés, P. (2010). Triple Percolation in Concrete Reinforced with Carbon Fiber. *ACI Materials Journal*, *107-M46*, 396-402.
- Banthia, N., Djeridane, S., & Pigeon, M. (1992). Electrical resistivity of carbon and steel micro-fiber reinforced cements *Cement and Concrete research - Pergamon Press Ltd.*, *22*, 804-814.
- Blunt, J., & Ostertag, C. P. (2009). Performance-Based Approach for the Design of a Deflection Hardened Hybrid Fiber-Reinforced Concrete. *Journal of Engineering Mechanics*, *135*(9), 978-986. doi:10.1061/(ASCE)0733-9399(2009)135:9(978)
- Blunt, J., & Ostertag, P. C. Deflection Hardening and Workability of Hybrid Fiber Composites. *Materials Journal*, *106*(3). doi:10.14359/56551
- Chen, B., Wu, K., & Yao, W. (2004). Conductivity of carbon fiber reinforced cement-based composites. *Cement and Concrete Composites*, *26*, 6.
- Chiarello, M., & Zinno, R. (2004). Electrical conductivity of self-monitoring CFRC. *Cement and Concrete Composites*, *27*.
- GAMRY-APN-1, G. (2015). *Application Note: Two-, Three-, and Four-Electrode Experiments*. Retrieved from
- GAMRY-APN-2, G. (2015). *Application Note: Potentiostat Fundamentals*. Retrieved from
- GAMRY-APN-3, G. (2015). *Application Note: Basics of Electrochemical Impedance Spectroscopy*. In. GAMRY-TUT-1, G. (2015). *Tutorials and Primers*. Retrieved from

- Han, B., Ding, S., & Yu, X. (2014). Intrinsic self-sensing concrete and structures: A review. *Measurement*, *59*, 18.
- Han, B., Guan, X., & Ou, J. (2006). Electrode design, measuring method and data acquisition system of carbon fiber cement paste piezoresistive sensors. *Sensors and Actuators A*, *135*.
- Han, B., Yu, X., & Ou, J. (2014). *Self-Sensing Concrete in Smart Structures*. The Boulevard, Langford Lane, Kidlington, Oxford OX5 1GB, UK & 225 Wyman Street, Waltham, MA 02451, USA: Butterworth-Heinemann.
- Hou, T.-C., & Lynch, J. P. (2005). Conductivity-based strain monitoring and damage characterization of fiber reinforced cementitious structural components. *Proceedings of SPIE 12th Annual International Symposium on Smart Structures and Materials, San Diego, CA, March 6-10, 2005*.
- Jen, G., Trono, W., & Ostertag, C. P. (2016). Self-consolidating hybrid fiber reinforced concrete: Development, properties and composite behavior. *Construction and Building Materials*, *104*, 63-71. doi:<http://dx.doi.org/10.1016/j.conbuildmat.2015.12.062>
- John S. Lawler, D. Z. a. S. P. S. Permeability of Cracked Hybrid Fiber-Reinforced Mortar under Load. *Materials Journal*, *99*(4). doi:10.14359/12220
- Konsta-Gdouts, M. S., & Aza, C. A. (2014). Self sensing carbon nanotube (CNT) and nanofiber (CNF) cementitious composites for real time damage assessment in smart structures *Cement and Concrete Composites*, *53*.
- Le, J.-L., Du, H., & Pang, S. D. (2014). Use of 2D Graphene Nanoplatelets (GNP) in cement composites for structural health evaluation. *Composites: Part B*.
- Liu, Q., Xu, Q., Yu, Q., Gao, R., & Tong, T. (2016). Experimental investigation on mechanical and piezoresistive properties of cementitious materials containing graphene and graphene oxide nanoplatelets. *Construction and Building Materials*.
- Markovich I, Van Mier J.G., & Walraven J.C. (2001). Single Fiber Pullout from Hybrid Fiber Reinforced Concrete. *Heron*, *46*(3).
- Meehan, D. G., Wang, S., & Chung, D. D. L. (2010). Electrical-resistance-based Sensing of Impact Damage in Carbon Fiber Reinforced Cement-based Materials. *Journal of Intelligent Material Systems and Structures*, *21*.
- Nemkumar Banthia, & Sayed Mohamad Soleimani. Flexural Response of Hybrid Fiber-Reinforced Cementitious Composites. *Materials Journal*, *102*(6). doi:10.14359/14800
- Ranade, R., Zhang, J., Lynch, J. P., & Li, V. C. (2014). Influence of micro-cracking on the composite resistivity of Engineered Cementitious Composites. *Cement and Concrete Research*, *58*, 12.
- Solgaard, A. O. S., Geiker, M., Edvardsen, C., & Kuter, A. (2013). Observations on the electrical resistivity of steel fibre reinforced concrete. *Materials and Structures*, *47*, 15.
- Teomete, E. (2014). Transverse strain sensitivity of steel fiber reinforced cement composites tested by compression and split tensile tests. *Construction and Building Materials*.
- Wen, S., & Chung, D. D. L. (2000). Damage monitoring of cement paste by electrical resistance measurement. *Cement and Concrete Research*, *30*.
- Wen, S., & Chung, D. D. L. (2003). A comparative study of steel- and carbon-fibre cement as piezoresistive strain sensors. *Advances in Cement Research*.
- Wen, S., & Chung, D. D. L. (2006). Self-sensing of flexural damage and strain in carbon fiber reinforced cement and effect of embedded steel reinforcing bars. *Carbon*, *44*, 1496–1502.
- Yeh, F.-Y., Chang, K.-C., & Liao, W.-C. (2015). Experimental Investigation of Self-Sensing Carbon Fiber Reinforced Cementitious Composite for Strain Measurement of an RC Portal Frame. *International Journal of Distributed Sensor Networks*, *2015*.
- Zhu, S., & Chung, D. D. L. (2007). Numerical assessment of the methods of measurement of the electrical resistance in carbon fiber reinforced cement. *Smart Materials and Structures*, *16*.